SYNTHESIS AND STRUCTURAL STUDY OF

AZIDONITROSYLBIS(TRIPHENYLPHOSPHINE)

NICKEL

Mrs. Nongnaphat Khosavithitkul

การสังเคราะห์ และศึกษาโครงสร้างของ
แอซิโดไนโตรซิลบิส(ไตรฟีนิลฟอสฟีน)นิเกิล

นางนงนภัส โฆษวิฑิตกุล

SYNTHESIS AND STRUCTURAL STUDY OF

AZIDONITROSYLBIS(TRIPHENYLPHOSPHINE)NICKEL

Suranaree University of Technology has approved this thesis submitted in partial fulfillment of the requirements for a Master's Degree.

Thesis Examining Committee

_____

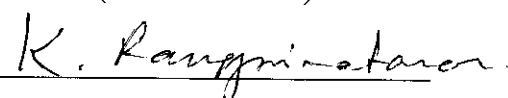(Asst. Prof. Dr. Malee Tangsathitkulchai)

Chairperson

_____

(Assoc. Prof. Dr. Kenneth J. Haller)
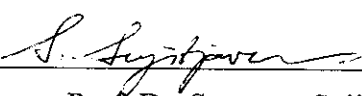
Member (Thesis Advisor)

_____

(Asst. Prof. Dr. Kunwadee Rangsriwatananon)

Member

_____

(Asst. Prof. Dr. Adrian E. Flood)

Member

_____   _____

(Assoc. Prof. Dr. Sarawut Sujitjorn)   (Assoc. Prof. Dr. Prasart Suebka)

Vice Rector for Academic Affairs   Dean of Institute of Science

นงนภัส โฆษวิฑิตกุล : การสังเคราะห์ และศึกษาโครงสร้างของแอซิโดไนโตรซิลบิส (ไตรฟีนิลฟอสฟีน)นิเกิล (SYNTHESIS AND STRUCTURAL STUDY OF AZIDONITROSYLBIS(TRIPHENYLPHOSPHINE)NICKEL) อาจารย์ที่ ปรึกษา : รองศาสตราจารย์ ดร.เค็นเนท เจ. แฮลเลอร์, 97 หน้า. ISBN 974-533-402-2

วิทยานิพนธ์นี้รายงานการสังเคราะห์ผลึกเชิงเดี่ยว $Ni(N_3)(NO)(PPh_3)_2$ และสามารถ ตรวจหาเอกลักษณ์อีกครั้งหนึ่งของโครงสร้างผลึกโดยเทคนิคเอกซ์เรย์คริสทัลโลกราฟี   ได้พบว่า ผลึกอยู่ในระบบมอโนคลินิกกลุ่ม $P2_1/c$ ประกอบด้วย $a = 13.597(5)$ Å, $b = 19.098(8)$ Å, $c = 12.562(4)$ Å, $\beta = 98.59(5)°$, $V = 3221.89$ Å^3, ที่อุณหภูมิ 298 เคลวิน นอกจากนี้ยังได้ศึกษา อันตรกิริยาของโครงสร้างซุปราโมเลคิวลาร์ของการเกาะกันของฟีนิลจำนวนมาก ทำให้เพิ่มความ เข้าใจโครงสร้างทางเคมีของผลึกนี้   ซึ่งพบว่า   อันตรกิริยาของพันธะไฮโดรเจนชนิดอ่อนของ C–H⋯O, C–H⋯N และ C–H⋯π   กับอิเล็กตรอนคู่โดดเดี่ยว และ ความหนาแน่นของ π อิเล็กตรอน ของกลุ่ม แอซิโด ไนโตรซิล และฟีนิล มีการเชื่อมต่อกันเกิดเป็นโครงสร้างซุปราโม เลคิวลาร์แบบสามมิติ

สารประกอบเชิงซ้อนแอซิโดมีระยะของ P⋯P ที่สั้นที่สุดเป็น 7.350 Å และ 7.783 Å, colinearity 86.9° และ 117.8° แต่ไม่เกิดอันตรกิริยาของ ซิกซ์โฟลดฟีนิลเอ็มบเรซ ซึ่งอันตร กิริยาของโซ่ที่แข็งแรงที่สุด เป็นอันตรกิริยาของ เอทโฟลดฟีนิลเอ็มบเรซ และ แพร์รัลเล็ลโฟโฟลด ฟีนิลเอ็มบเรซ ซึ่งเกี่ยวข้องกับ C–H⋯N ทั้ง 4 ขณะที่อันตรกิริยาของ nonbonded ที่แข็งแรง ที่สุด 2.466   Å เป็นอันตรกิริยาภายในโมเลกุลของ   C–H⋯N ที่อิเล็กตรอนคู่โดดเดี่ยวของ ไนโตรเจนที่เกาะกับนิเกิล   รวมทั้งยังมีอันตรกิริยาของวงฟีนิลและอันตรกิริยาซึ่งเกี่ยวข้องกับ C–H⋯N   ที่เชื่อมต่อกันเกิดเป็นโครงสร้างแบบสามมิติ ดังนั้นลิแกนด์แอซิโดกลายเป็นส่วนที่ สำคัญที่กำหนดโครงสร้างผลึกของสารประกอบเชิงซ้อนแอซิโดที่แผ่ขยายออกไป

สาขาวิชาเคมี   ลายมือชื่อนักศึกษา _K. Kosgnaphat_
ปีการศึกษา 2547   ลายมือชื่ออาจารย์ที่ปรึกษา _Kenneth J Haller_

NONGNAPHAT KHOSAVITHITKUL : SYNTHESIS AND STRUCTURAL STUDY OF AZIDONITROSYLBIS(TRIPHENYLPHOSPHINE)NICKEL. THESIS ADVISOR : ASSOC. PROF. KENNETH J. HALLER, Ph.D. 97 PP. ISBN 974-533-402-2

SUPRAMOLECULAR STRUCTURE/AZIDO/NITROSYL

This thesis reports syntheses of $Ni(N_3)(NO)(PPh_3)_2$, and redetermination of the single crystal X-ray structure based on a data set collected on a KappaCCD diffractometer to improve the model for the azide region. The deep blue-black crystals are monoclinic, $P2_1/c$, with unit cell parameters at 298 K of $a = 13.597(5)$ Å, $b = 19.098(8)$ Å, $c = 12.562(4)$ Å, $\beta = 98.59(5)°$, $V = 3221.89$ Å^3, and Z = 4. The discrete pseudo tetrahedral molecules are interconnected into a three-dimensional supramolecular structure by concerted C$-$H$\cdots$O, C$-$H$\cdots$N, and C$-$H$\cdots\pi$ hydrogen bonds to the lone pair and π electron density of the azido, nitrosyl, and phenyl groups.

The shortest intermolecular P$\cdots$P distances in the azido complex are 7.350 Å and 7.783 Å with colinearities of 86.9° and 117.8°, thus not sixfold phenyl embraces. A stronger chain of alternating eightfold phenyl embraces and parallel fourfold phenyl embraces supplemented by four C$-$H$\cdots$N interactions occurs. Also, the strongest nonbonded interaction is the 2.466 Å *intra*molecular C$-$H$\cdots$N interaction to the lone pair on the azido N bonded to Ni. There are several phenyl-phenyl interactions as well as other C$-$H$\cdots$N interactions linking the chains into a three-dimensional network. The azido ligand, thus becomes a dominant influence in determining the extended crystal structure.

School of Chemistry   Student's Signature _____

Academic Year 2004   Advisor's Signature _____

ACKNOWLEDGEMENTS

Nongnaphat Khosavithitkul

CONTENTS

CONTENTS (Continued)

LIST OF TABLES

LIST OF TABLES (Continued)

LIST OF FIGURES

LIST OF FIGURES (Continued)

LIST OF SYMBOLS AND ABBREVIATIONS

Symbols

···	noncovalent interaction or nonbonded interatomic separation
−	primarily covalent interaction or coordination interaction
−H···	hydrogen bond interaction
∠[−]	interplanar dihedral angle
∠[− −]	interatomic angle for normal bonded atoms
∠[− ···]	interatomic angle involving a noncovalent interaction
∠[− − −]	interatomic torsional angle
α, β, γ	unit cell angles
θ	Bragg angle or scattering angle
λ	wavelength of x-radiation
μ	linear absorption coefficient
ρ	electron density
a, b, c	unit cell dimensions
d[−]	interatomic bond distance for normal bonded atoms
d[···]	interatomic bond distance for a noncovalent interaction
U[ ]	isotropic atomic displacement parameter for the indicated atom
z	charge on an ionic species
Z	number of formula units in the unit cell or atomic number of an atom

LIST OF SYMBOLS AND ABBREVIATIONS (Continued)

Abbreviations

1-D	one-dimensional
2-D	two-dimensional
2PE	twofold phenyl embrace
3-D	three-dimensional
4AE	fourfold aryl embrace
4PE	four-fold phenyl embrace
6AE	sixfold aryl embrace
6PE	sixfold phenyl embrace
ACS	American Chemical Society
ADC	Atom Designator Code
ADR	Atom Designator Run
ANR	Atom Number Run
ATI	aminotroponiminate
Bz	benzene
CSD	Cambridge Structure Database of organic crystal structures.
DPE	Double Phenyl Embrace
ee	Edge-to-Edge interaction
ef	Edge-to-Face interaction
EvalCCD	data reduction software from Bruker Nonius
ff	Face-to-Face interaction
FTIR	Fourier transform infrared spectroscopy

LIST OF SYMBOLS AND ABBREVIATIONS (Continued)

Abbreviations

gof	estimated standard deviation of an observation of unit weight, or goodness of fit
HA6PE	hexagonal array of sixfold phenyl embrace
HASPE	hexagonal array of sextuple phenyl embrace
ins	file name extension of SHELX instruction input file
ISO	International Standards Organization
kV	kilovolts
kJ	kilojoules
mA	milliamperes
NNTTTSS	*atom designator code (ADC)*
off	Offset Face-to-Face interaction
O4PE	Orthogonal fourfold phenyl embrace
O8PE	Orthogonal eightfold phenyl embrace
OQPE	Orthogonal Quadruple Phenyl Embrace
ORTEP	Oak Ridge Thermal Ellipsoid Plot program
OSPE	Offset Sextuple Phenyl Embrace
P4PE	Parallel fourfold phenyl embrace
P8PE	Parallel eightfold phenyl embrace
P12PE	Parallel twelvefold phenyl embrace
PQPE	Parallel Quadruple Phenyl Embrace
Ph	phenyl group (C_6H_5)

LIST OF SYMBOLS AND ABBREVIATIONS (Continued)

Abbreviations

Pr	propyl
R_1	conventional crystallographic discrepancy index
RPE	Analytical Grade Reagent
SD	standard deviation
SEM	scanning electron microscope
SHELXL97	least squares structure refinement program
SIR97	direct methods structure solution software
SPE	Sextuple Phenyl Embrace
trpn	3,3`,3``-Triaminotripropylamine
tren	(2-aminoethyl)amine
VDC	Vector Designator Code
vf	Vertex-to-Face interaction
wR_2	Weighted crystallographic discrepancy index
ZZI6PE	zig-zag infinite sixfold phenyl embrace
ZZISPE	zig-zag infinite sextuple phenyl embrace
hkl	Designate lattice point or "reflection"
(*hkl*)	Designate lattice planes or crystal faces

CHAPTER I

INTRODUCTION

1.1 Overview

Four-coordinate nickel complexes have been studied for many years, partially due to the small energy difference between the square planar and tetrahedral limiting geometries (Venanzi, 1958) and the ease of distinguishing the two geometries by their magnetic behaviors. Nickel phosphine complexes exhibit catalytic activity in the cross-coupling of Grignard reagents with aryl and alkyl halides (Cotton, Willkinson, Murillo & Bochmann, 1999). Some of the most effective catalysts employed as selective hydrogenation, isomerization, and hydroboration catalysts contain triphenylphosphine complexes such as dichlorobis(triphenylphosphine)nickel(II) (Palo & Erkey, 1998). At the same time there has been an increase of interest in the study of nitrosyl chemistry because of biological implications (Stamler & Feelisch, 1996). Nickel and nitrosyl are interesting in that both exhibit variable stereochemistry due to electronic and/or steric effects. Nickel(I) and nickel(II) species are being studied increasingly because of the possible involvement of these oxidation states in nickel-containing metalloenzymes.

The four-coordinate complexes of nickel have either square planar or tetrahedral limiting geometries. The d^8 configuration is ideal for the formation of low spin square planar complexes with strong field ligands, which for nickel(II) complexes are typically red or yellow. The tetrahedral high spin complexes are typically formed with bulky ligands such as triphenylphosphine, triphenylphosphine

oxide, or weaker field ligands such as the halides. Tetrahedral nickel(II) complexes are typically deep blue or green-blue resulting from an intense absorption band (Huheey, Keiter & Keiter, 1993). Depending on the ligands, the balance can be shifted and complexes isolated as tetrahedral or square planar forms. In one example, the dibromobis(benzyldiphenylphosphine)nickel(II) complex crystallizes with both tetrahedral and square planar forms coexisting in the same crystal lattice (Kilbourn & Powell, 1970).

Conventionally, metal-phosphine bonding has been described as a ligand to metal σ bond plus metal to ligand π back bond using the acceptor character of the empty $3d$ orbitals on the phosphorus atom. Orpen and Connelly (1985) used structural data to confirm the theoretical studies (Xiao, Trogler, Ellis & Berkovich-Yellin, 1983) suggesting that the σ* phosphine orbitals are π-acid in character and act as the π-acceptor for the metal d electron back bond. The changes in M−P and P−C bond lengths in a series of reduction-oxidation related pairs of transition metal phosphine complexes are consistent with M−P bonding in the complexes containing an important π-component from metal $3d$ to ligand σ*. Brammer and Stevens (1989) note the significant shortening of the P−C bonds in the $NiCl_2(PPh_3)_2$ complex, consistent with a π back-bonding model incorporating P−C σ* orbitals in the acceptor role, and also the possibility of Jahn-Teller distortion in nickel(II) complexes (as compared to nickel(II) metal ion).

Another stereochemically flexible moiety that has been studied extensively is the metal nitrosyl triatomic fragment. The properties of $\{MNO\}^{10}$ complexes should be sensitive to the stereochemistry about the metal atom, and two limiting possibilities have been proposed for four-coordinate complexes containing the

{MNO}^{10} moiety: pseudo tetrahedral geometry with a linear MNO group, and square-planar geometry with a strongly bent MNO group (Enemark & Feltham, 1974). Intermediate distorted coordination geometries should have intermediate NiNO angles (Haller & Enemark, 1978).

The relationship between the Ni−N−O bond angle and the nickel coordination geometry in the low symmetry {NiNO}^{10} complexes[1] of the general formula NiX(NO)L$_2$, where X is a monoanion and L is a triphenylphosphine have been probed. The complexes were expected to have tetrahedral structures on the basis of their large dipole moments. Previous studies (Enemark, 1971; Haller & Enemark, 1978) have shown the X = azido, chloro, and isothiocyanato complexes to have a distorted tetrahedral geometry.

Metal complexation and supramolecular recognition of the polyfunctional azide anion is extremely important in biochemistry. The coordination of azide anion by metal atoms in coordination compounds gives rise to a redistribution of the anionic charge in the azide ligand, which in turn, controls the hydrogen-bonding acceptor properties of the azide nitrogen atoms. The bonding in covalent azides can generally be understood in terms of the two forms, I and II, with the relative importance of each form dependent upon the substituent R. Changes in the electronic properties of R are reflected in changes in the N−N bond distances, and in this regard X-ray crystallography provides a valuable tool in assessing substituent effects in covalent azides (Zigler, Haller, West & Gordon, 1989).

---

[1] The {MNO}^{n} notation is used herein to avoid ambiguity in assigning formal oxidation states in metal nitrosyls. The n corresponds to the total number of metal d and nitrosyl π* electrons in the complex for nitric oxide assumed to be coordinated as (N≡O)$^+$ (Enemark, Feltham, Riker-Nappier & Bizot, 1975).

$$\underset{R}{N}\!\!=\!\!N^+\!\!=\!\!N^-$$

I

$$\underset{R}{N^-}\!\!-\!\!N^+\!\!\equiv\!\!N$$

II

When the azide ion coordinates to a metal as a two-electron donor there are two possible Lewis structures for the resulting fragment, and the third possibility of a resonance hybrid:

$$\underset{M}{:\!N}\!\!=\!\!N^+\!\!=\!\!\ddot{N}\!\!:\!\!^-$$

III

$$\underset{M}{:\!\ddot{N}^-}\!\!-\!\!N^+\!\!\equiv\!\!N\!:$$

IV

$$\underset{M}{N}\!\!=\!\!=\!\!=\!\!N\!\!=\!\!=\!\!=\!\!N$$

V
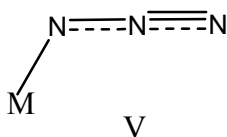
In case (III) the coordinating N is sp^2 hybridized, the ideal M−N−N angle is 120º, and d[N1−N2] and d[N2−N3] should be nearly equal. In case (IV) the coordinating N is sp^3 hybridized, the ideal M−N−N angle is 109º, and d[N1−N2] and d[N2−N3] should be single bond and triple bond distances, respectively. The resonance hybrid (V) should have an angle intermediate between the angle in case (III) and the angle in case (IV), and distances intermediate between those for case (III) and those for case (IV), and in any event with d[N1−N2] longer than d[N2−N3]. This description does not take into account possible metal to ligand back bonding.

The reported $Ni(N_3)(NO)(PPh_3)_2$ structure (Enemark, 1971), exhibits distorted, pseudo tetrahedral geometry ($\angle$(P−Ni−P) = 120.5°; $\angle$((N$_3$)−Ni−NO) = 128.8°;

NiP_2-NiN_2 dihedral angle = 85.1°) with bent azide ($\angle(Ni-N-N)$ = 128.1°, $d[Ni-N_3]$ = 2.018 Å) and bent nitrosyl ($\angle(Ni-N-O)$ = 152.7°, $d[Ni-NO]$ = 1.686 Å). Surprisingly, the $\angle[Ni-N1-N2]$ = 128.1° is outside the expected range, and the $d[N-N]$ at $d[N1-N2]$ = 0.98 Å and $d[N2-N3]$ = 1.28 Å, are in the opposite order to that expected from the resonance analysis above. Perhaps even more surprising is the extreme shortness of $d[N1-N2]$ in the reported structure.

Furthermore, although not of direct interest in this study, another interesting feature in this complex is that the chemically equivalent Ni−P bonds are distinctly nonequivalent. The author suggested the nonequivalence could result from the nonlinear geometry of the coordinated azide which might induce inequivalent electronic environments for the two phosphine ligands. However, the pattern of long and short Ni−P distances was counter to that argument. The isothiocyanato complex, $Ni(NCS)(NO)(PPh_3)_2$, reported soon thereafter (Haller & Enemark, 1978) which contains linearly coordinated NCS^- ligand also exhibits nonequivalent Ni−P bonds, thus dispelling this steric explanation. Other suggestions of the cause were the possibility that the nonequivalence was the result of vibronic distortions of the molecule, or that they could result from packing effects (supramolecular structure) (Haller, 1978).

A recent search in the Cambridge Structural Database (2001), the CSD, for small molecule crystal structures containing the metal-azide group found 270 structure reports, with 22 structure reports, including the $Ni(N_3)(NO)(PPh_3)_2$ complex noted above, for the fragment consisting of four-coordinate nickel bound to azide (Tchertanov, 2000). Table 1.1 shows examples of structural azide complexes.

Table 1.1. M−NNN Geometry in Selected Complexes.

Azide complexes	Geometry	M···N (Å)	∠(MN1N2) (°)	N1−N2 (Å)	N2−N3 (Å)	Reference
[CuL^a(N$_3$)(ClO$_4$)]$_n$	Octahedral	1.954(3)	126.9(4)	1.171(6)	1.134(6)	Manikandan, P.; *et al.*, 2001.
[Cu(trpn)(N$_3$)]ClO$_4$	Distorted Square Pyramidal	2.044(5)	130.9	1.184(7)	1.145(7)	Massoud, S. S.; *et al.*, 1999.
[Ti(NMe$_2$)$_2$(N$_3$)$_2$bipy]	Octahedral	2.067(5)	132.3(4)	1.197(7)	1.148(8)	Carmalt, C. J.; *et al.*, 1997.
[Ti(NMe$_2$)$_2$(N$_3$)$_2$(py)$_2$]	Octahedral	2.075(3)	133.4(3)	1.183(4)	1.135(5)	Carmalt, C. J.; *et al.*, 1997.
[Ti(NMe$_2$)$_3$(N$_3$)bipy]	Octahedral	2.150(5)	133.7(5)	1.194(7)	1.163(7)	Carmalt, C. J.; *et al.*, 1997.
Molecule 2 of [(n-Pr)$_2$ATI]SnN$_3$	Pyramidal	2.230(5)	119.1(3)	1.105(6)	1.177(6)	Ayers, A. E.; *et al.*, 2000.
[Cd(4-Acpy)$_2$(N$_3$)$_2$]$_n$	Octahedral	2.326(4)	120.5(3)	1.184(6)	1.183(7)	Goher, M. A. S.; *et al.*, 2002.

a: L=2,6-(pyrazol-1-ylmethy) pyridine

One possible explanation for the short d[N1−N2] distance, suggested by the elongated atomic displacement parameter of N2 oriented along the azido ligand axis, (Figure 1.1), is that the unreasonably short N1−N2 bond and the oriented elongated atomic displacement parameters are the result of unreacted chloro complex starting material cocrystallized in the azide lattice. While this possibility was noted (Enemark, 1971), no attempt was made to model such a disorder.
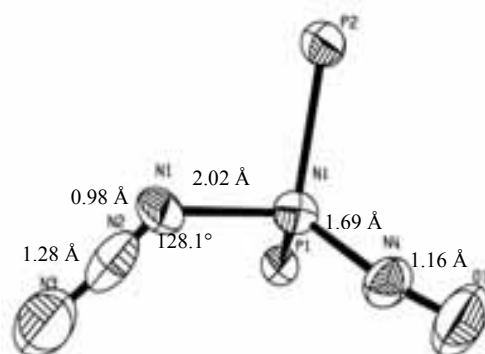
Figure 1.1. Perspective view of the inner coordination sphere of Ni(N$_3$)(NO)(PPh$_3$)$_2$. Parameters from Enemark (1978).

Interestingly, the closely related NiCl(NO)(PPh$_3$)$_2$ complex reported a few years later (Haller, 1978; Haller & Enemark, 1978), gives additional insight into the posited disorder. In the chloro-nitrosyl structure, the two ligands have nearly the same number of electrons (17 and 15, respectively) and the Ni−Cl, Ni−N, and N−O bond lengths are such that the midpoint of the N−O vector and the Cl atom position can be nearly superposed by the pseudo 2-fold axis defined by the Ni(PPh$_3$)$_2$ portion of the molecule. Details of the disorder modeling of the chloro and nitrosyl ligands in NiCl(NO)(PPh$_3$)$_2$ were reported (Haller, 1978).

The azido nitrosyl under consideration here may suffer a similar fate if the metathesis reaction does not reach completion. The unreacted starting material impurity may cocrystallize with the azido complex giving crystals with substitutional disorder with the azido ligand and the chloro ligand occupying the same relative position in the lattice. The posited overlap is shown in Figure 1.2.
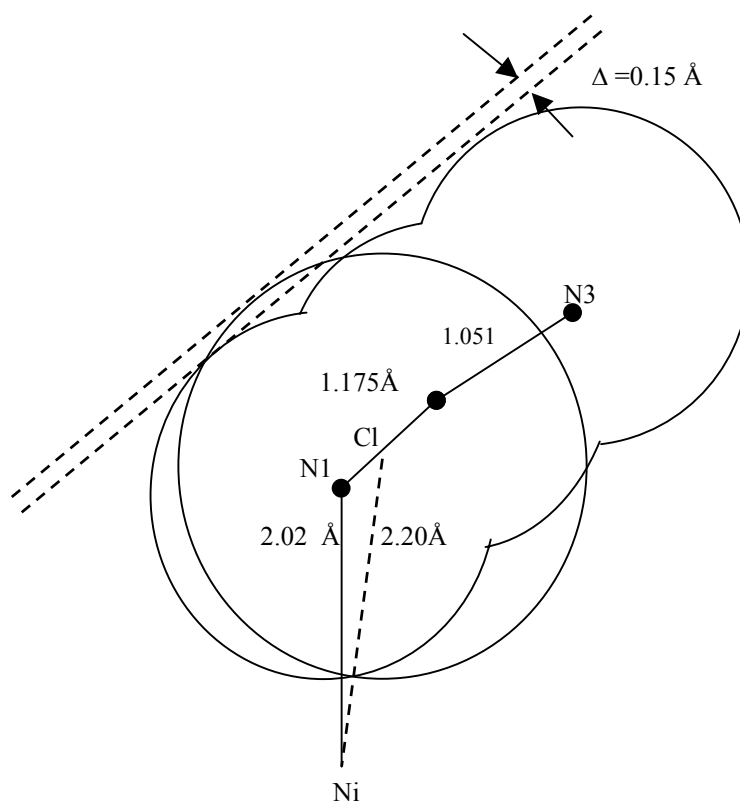
Figure 1.2. Possible substitutional disorder model for N2 and Cl atoms of impure $Ni(N_3)(NO)(PPh_3)_2$.

A possible solution to this problem, at least for the $Ni(N_3)(NO)(PPh_3)_2$ complex, would be to alter the synthetic route, going through the bromo precursor rather than the chloro precursor. The bromo ligand is slightly weaker field, and should be a better leaving group, thus making it more likely that the metathesis reaction reaches completion. Furthermore, d[Ni–Br] = 2.35 Å, and the van der Waals radius of bromine = 1.85 Å, are larger than the chloro values by 0.15 Å and 0.10 Å, respectively. The combined effects make a coordinated bromo group (Figure 1.3) significantly larger than the azido group (about 0.4 Å), making it less likely that a bromo impurity would cocrystallize with the azido complex.
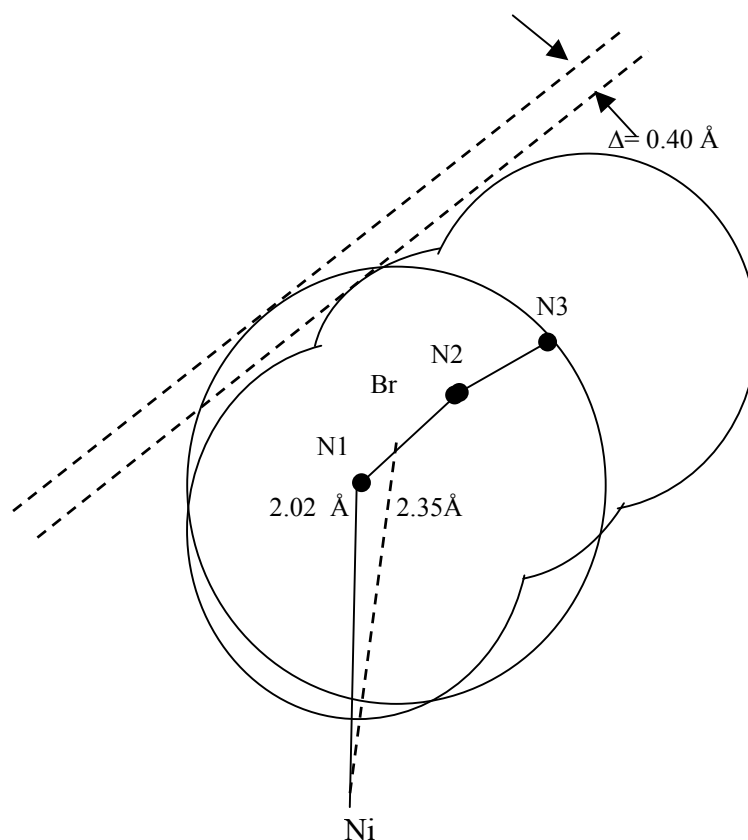
Figure 1.3. Model similar to the possible substitutional disorder suggested for chloro complex in the presence of azido complex if Cl is changed to Br.

The supramolecular structures of the three previously determined low symmetry $Ni(X)(NO)(PPh_3)_2$ complexes which have geometry intermediate between square planar and tetrahedral were recently reexamined (Kiatpichitpong, 2002). It was expected that the packing of these complexes would be dominated by the six-fold phenyl embraces (6PE) recently described by Dance and Scudder (1995) and found to be present in 95% of bis(triarylphosphines). The expected 6PE motif was found as the dominant supramolecular feature in the isothiocyanato complex. The 6PE motif was also found in the chloro complex, but the benzene of crystallization seemed to be more important in determining the supramolecular structure.

The azido complex, however, does not exhibit the expected 6PE motif, and the azido group appeared to be the most important determiner of the supramolecular structure. The analysis of the strongest C−H···N interactions reported by Kiatpichitpong is straightforward, but the concerted weaker interactions eluded systematic characterization.

Tchertanov (2000) suggested that there are five types of H-bonding for azide, each having a different structure:

  (i) by only the terminal nitrogen atom;

 (ii) by only the nitrogen atom bonded to the metal;

(iii) by the nitrogen atoms on both azide ends;

(iv) by the central azide nitrogen atom;

 (v) twice through one of the terminal atoms.

These appear to be based primarily on valence bond ideas; (i) (ii) (iii) & (iv) are based mostly on lone pair ideas, and (v) is based mostly on the pi-bond electron clouds.

The current work reports a new synthesis of the $Ni(N_3)(NO)(PPh_3)_2$ complex from a bromo precursor, an improved X-ray structure determination of the complex, and a systematic analysis of the supramolecular structure based on the weak noncovalent C−H···N, C−H···O, and C−H···π interactions.

CHAPTER II

THEORETICAL BACKGROUND

2.1 Background of Azide

Azide is a small, electron rich, linear, triatomic, monoanion wherein the negative charge can be localized on one of the terminal atoms or delocalized over the whole anion, as shown in the following resonance forms:

$$\ominus\ddot{N}=\ddot{N}-\ddot{N} \quad\longleftrightarrow\quad \ddot{N}-\ddot{N}=\ddot{N}\ominus$$

$$N\equiv\overset{\oplus}{N}-\ddot{N}{:}^{2-} \quad\longleftrightarrow\quad {}^{2-}{:}\ddot{N}-\overset{\oplus}{N}\equiv N{:}$$
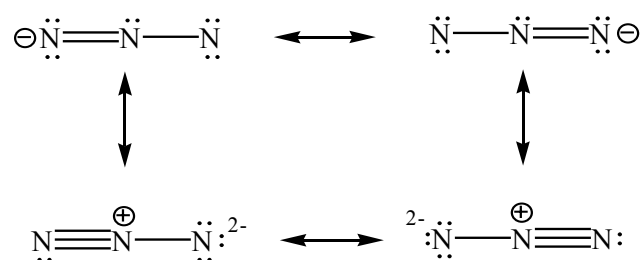
It can occur in crystal structures in the discreet monoanionic form or bonded to metals or main group elements. Azide can coordinate with transition metals as either a monodentate or a bidentate ligand offering different modes of binding with metals through one of the terminal nitrogen atoms (one time, I, or two times, bridging mode II) or through both of the terminal nitrogen atoms (bridging mode III) (Cotton, Wilkinson, Murillo & Bochmann, 1999).
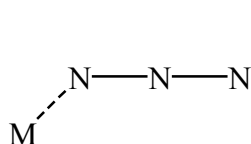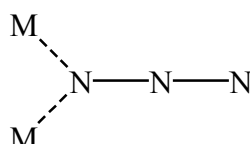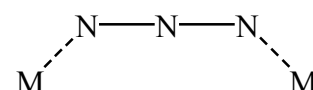
| I | II | III |

Table 2.1 gives average parameters for the five types of azide/azido groups as determined from the structure databases.

Table 2.1. Mean Values of the Geometrical Parameters for the Various Azide Geometries.

Parameter[a]	Anionic Azide	Interaction Mode[b]			
		I	II	III	R[c]
N1−N2 (Å)	1.158(5)	1.175(2)	1.202(5)	1.170(4)	1.220(3)
N2−N3 (Å)	1.159(5)	1.151(2)	1.149(7)	1.171(3)	1.130(2)
N1···N3 (Å)	2.317(7)	2.325(3)	2.351(7)	2.370(5)	2.344(3)
∠(N1N2N3) (º)	179.0(3)	176.0(2)	178.0(3)	177.6(2)	172.5(2)
M−N1 (Å)		2.050(8)	2.12(2)	2.18(2)	1.51(1)
M−N3 (Å)				2.18(3)	
∠(MN1N2) (º)		126.4(5)	124.7(7)	131(2)	115.9(2)
∠(MN3N2) (º)				131(2)	
N obs	19	270	109	50	208

a. Numbers given in parentheses are the standard deviations in the least significant digits.
b. A definition of interaction modes is given in the text. (Tchertanov, 2000).
c. R = C, B, P, Si, and I in R−NNN compounds.

2.2 Supramolecular Chemistry

In recent years supramolecular chemistry has established itself as one of the most active fields of science. Pioneering work in this field was reported by Cram and Cram (1974), Lehn (1973), and Pedersen (1967). Their work is mainly on crown ethers and cryptands in the area of host-guest chemistry and has been awarded the 1987 Nobel prize in chemistry. Early inspiration for the construction of supramolecular species was obtained from nature and especially from biological aggregates like lipid bilayers, viral capsids, the DNA double helix, and the tertiary

and quaternary structure of proteins (Klug, 1983). Nowadays the area of supramolecular chemistry stretches from molecular recognition in natural and artificial complexes to applications in such diverse areas as new materials, biology, chemical technologies, or medicine. The most important feature of supramolecular chemistry is building blocks which are reversibly held together by intermolecular forces (noncovalent self-assembly). The reversible formation under thermodynamic control allows correction that may occur during the self-assembly process. However the outcome may still be difficult to control (Bein, 1992).

Supramolecular chemistry is defined as chemistry based on noncovalent interactions, such as hydrogen bond, dipole-dipole, dipole-induced dipole, electrostatic, charge-transfer, hydrophobic, dispersive van der Waals, and coordination interactions. Lehn (1995) wrote the definition: "*Supramolecular chemistry* is chemistry beyond the molecule, whose goal is to gain control over the intermolecular noncovalent bond. It is concerned with the entities of higher complexity than molecules themselves. Supramolecular species and assemblies held together and organized by means of intermolecular, binding interactions. It is a highly interdisciplinary field of science and technology, bridging chemistry with biology and physics."

Supramolecular science comprises aspects of synthetic chemistry, physical chemistry, molecular physics, biochemistry and biophysics, materials engineering, and nanoelectronics. Development of supramolecular chemistry evolved into two general mainstreams: biomimetics dealing with artificial systems mimicking natural processes and phenomena, and self-organization, dealing with the formation of well-defined molecular entities, often of nanometric size. It can be justified that the further

consequence of self-organization was the development of the new scientific field nanoscience, that was inspired in a large part from supramolecular science (Andres & Schubert, 2003), even though nanoscience goes well beyond the scope of supramolecular science. Nanoscience and nanotechnology are also based on nanometric entities of metals, insulators, biomaterials, and semiconductors, whose electronic properties are very different from the materials in the bulk (Gohy, Lohmeijer & Schubert, 2003). Both, supramolecular science and nanoscience and nanotechnology open unlimited horizons for new scientific and technological discoveries in fields associated with environmental protection, health protection, electronics, telecommunications, sustainable energy sources (advanced photovoltaics), and the fight with organized crime and international terrorism. These disciplines enjoy particularly strong funding and government initiatives in the developed countries (Jones & Rao, 2002).

In contrast to the covalent nanostructures, self-assembled supramolecules use multiple weak interactions which act cooperatively combining metal ligation, hydrogen bonding, π-π stacking, dipolar interaction, van der Waals forces, and hydrophobic interactions to hold molecular components together (Beer, Gale & Smith, 1999). These are the same forces that Nature uses to bind its molecular assemblies (Constable, 1991).

One of the most important aspects of supramolecular chemistry is the understanding and the ability to exploit noncovalent interactions for the controlled and reversible assembly of functional entities. The term "noncovalent" contains an enormous range of intermolecular interactions, which originate from only a few attractive and repulsive forces. These are in order of decreasing strength:

(i)   electrostatic interactions (ion-ion, ion-dipole and dipole-dipole interactions) and coordinative bonding (metal-ligand);

(ii) hydrogen bonding;

(iii) aromatic-aromatic interaction;

(iv) van der Waals forces (Schneider & Yatsimirsky, 2000; Steed & Atwood, 2000).

Noncovalent Interactions

Weak noncovalent interactions have a constitutive role in biological or biomimetic systems as well as in artificial supramolecular structures. Although van der Waals interactions were first recognized by J. D. van der Waals in the nineteenth century (Müller-Dethlefs & Hobza, 2000), their role in nature has been unravelled only during the past two decades.

In contrast to the covalent interactions that dominate in classical molecules, noncovalent interactions are weak interactions that bind different kinds of building blocks together into supramolecular entities (Schneider & Yatsimirsky, 2000). Covalent bonds are generally shorter than two Ångstroms, while noncovalent interactions function within a range of several Ångstroms. The formation of a covalent bond requires overlapping of partially occupied orbitals of interacting atoms, which share a pair of electrons. In noncovalent interactions, no orbital overlap is necessary because the attraction comes from the electrical properties of the building blocks.

The noncovalent interactions involved in supramolecular entities may be a combination of several interactions, *e.g.* ion-pairing, hydrogen bonding, cation−π,

π−π interactions, *etc*. (Steed & Atwood, 2000; Lehn, 1995; Müller-Dethlefs & Hobza, 2000; Schneider & Yatsimirsky, 2000; Bianchi, Bowman-James & Garcia-Espana, 1997). A wide range of attractive and repulsive forces is included under the term noncovalent. Noncovalent interactions comprise interactions between permanent multipoles, between a permanent multipole and an induced multipole, and between a time-variable multipole and an induced multipole. The stabilizing energy of noncovalent complexes is generally said to consist of the following energy contributions: electrostatic (or Coulombic), induction, charge transfer, and dispersion. These terms are basically attractive terms. The repulsive contribution, which is called exchange-repulsion, prevents the subsystems from drawing too close together. The term induction refers to the general ability of charged molecules to polarize neighboring species, and dispersion (London) interaction results from the interactions between fluctuating multipoles. In charge-transfer interactions the electron flow from the donor to the acceptor is indicated. The term van der Waals forces is frequently used to describe dispersion and exchange-repulsion contributions, but sometimes also other long-range contributions are included in the definition. All of these interactions involve host and guest as well as their surroundings (*e.g.* solvation, crystal lattice, and phase).

Electrostatic Interactions

In ion pairing (ion-ion, ion-dipole, dipole-dipole, and dipole-induced dipole) the driving force is electrostatic interactions, which unquestionably play an important role in natural and in supramolecular systems (Steed & Atwood, 2000; Schneider & Yatsimirsky, 2000). Charges are heavily delocalized in organic ions, which

complicates the theoretical analysis of ion pairing (Schneider & Yatsimirsky, 2000; Bianchi, Bowman-James & Garcia-Espana, 1997). As a means to understand ion pairs, theoretical approaches to the association constant (K) based on Debye-Hückel theory have been developed by Bjerrum (spherical ions with point charges) and Fuoss (contact ion pairs) (Hossain & Schneider, 1999). A numerical method introduced by Poisson permits the consideration of solvent molecules, and the salt effect is well described by Manning's counterion condensation theory (Schneider & Yatsimirsky, 2000; Hossain & Schneider, 1999). The interaction of the organic cation tris(diazabicyclooctane) with $Fe(CN)_6^{3-}$ is an example of supramolecular ion-ion interaction (Steed & Atwood, 2000). The structure of an alkali metal cation with a macrocyclic crown ether is an example of a supramolecular ion-dipole interaction. In the latter case the lone electron pairs on the oxygen atoms are attracted to the positive charge of the cation. Between neutral polar molecules the electrostatic contributions come mostly from dipole-dipole interactions

Hydrogen Bonding

Hydrogen bonding is a relatively strong and probably the most important noncovalent interaction (Steed & Atwood, 2000; Müller-Dethlefs & Hobza, 2000; Bianchi, Bowman-James & Garcia-Espana, 1997). Hydrogen bonded complexes are stabilized by electrostatic, induction, and dispersion energy terms. The electrostatic term is contributed by dipole-dipole and ion-dipole interactions, which give hydrogen bonds their highly directional nature. A hydrogen bond, D−H⋯A, is formed between an electronegative donor atom (D) with an attached hydrogen atom and a neighboring acceptor atom (A). Different types of H-bonds are presented in Figure 2.1 where the

last two types are less frequent than the first two types (Schneider & Yatsimirsky, 2000). Properties and a common classification of the H-bonds in terms of strength are represented in Table 2.2. The concept of hydrogen bonding has also been extended to the weaker C−H⋯O type, which has been studied systematically only recently (Steiner, 1997; Steiner & Desiraju, 1998).
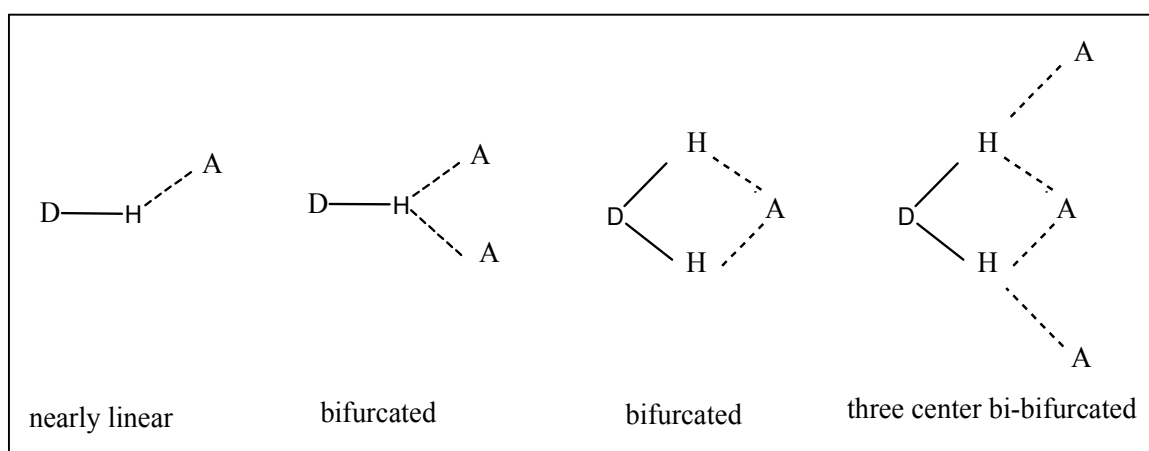
Figure 2.1. Schematic diagram of hydrogen bonds. D represents a donor atom and A represents an acceptor atom.

Table 2.2. Classification and Some Properties of Hydrogen Bonds[a].

D–H···A	Strong	Moderate	Weak
interaction	Mainly covalent	Mainly electrostatic	Electrostatic
Bond energy (KJ mol^{-1})	60-120	16-60	< 12
H···A length (Å)	1.2-1.5	1.5-2.2	2.2-3.2
D···A length (Å)	2.2-2.5	2.5-3.2	3.2-4.0
D−H···A angle (°)	175-180	130-180	90-150
Examples	gas phase dimers with strong acids/bases, HF complexes	acids, biological molecules	C−H···N/O and N/O−H···π hydrogen bonds

a. Steed & Atwood, 2000

Cation–π Interaction

In cation−π interactions surprisingly strong forces are found between cations and a π face of an aromatic structure (Steed & Atwood, 2000; Müller-Dethlefs & Hobza, 2000; Schneider & Yatsimirsky, 2000). Electrostatic forces appear to play the dominant role in the cation−π interaction, though modern theories also involve additional terms such as induced dipoles, polarizability, dispersion, and charge transfer. The charge distribution of a benzene type aromatic is illustrated in Figure 2.2. The offsetting dipoles in free benzene are indicated by the arrows to the right.
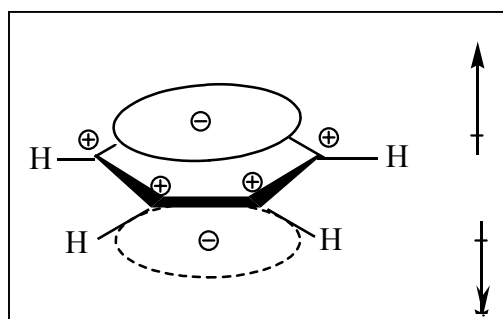
Figure 2.2. The charge distribution in benzene. The δ+ due to the hydrogen atoms and the δ− due to the negatively charged π-electron cloud are indicated.

Aromatic π−π Interaction

Weak electrostatic, π−π interactions occur between aromatic moieties (Steed & Atwood, 2000; Schneider & Yatsimirsky, 2000; Ma & Dougherty, 1997; Hunter & Sanders, 1990). The stabilizing energy of π−π interactions also includes induced dipole and dispersion contributions. Two general types of aromatic π−π interactions are face-to-face, *ff*, and edge-to-face, *ef*, (Figure 2.3(a), are actually C−H···π type interactions (the C−H bond generally having a small dipole moment), the attraction coming from the interaction between positively charged hydrogen atoms and the negatively charged π-face of the aromatic system. Perfect facial alignment of the *ff* orientation is unlikely because of the electrostatic repulsion between the two negatively charged π-systems of aromatic rings (Figure 2.3(b). The distance between the aromatic π−π faces is about 3.3−3.8 Å (Nishio & Hirota, 1989, Steiner, 1998).

face-to-face

edge-to-face

(a)

(b)
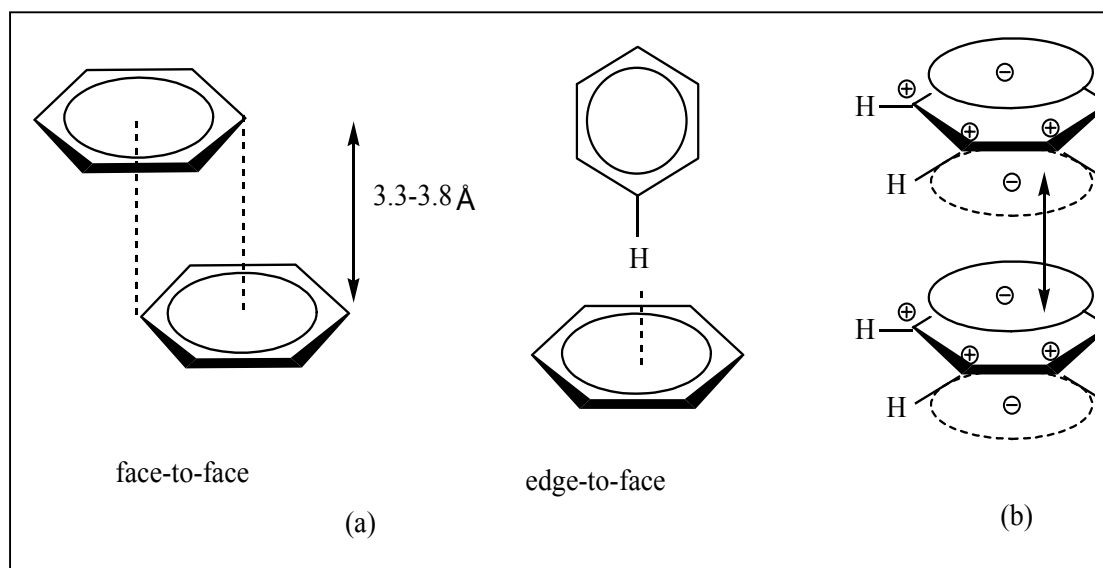
Figure 2.3. Limiting types of aromatic π−π interactions. (a) *ff* (interplanar distance about 3.3−3.8 Å) and *ef* orientations. (b) Repulsion between negatively charged π−electron clouds of perfectly eclipsed oriented aromatic rings.

Multiple Phenyl Embraces

Crystal structures of triphenylphosphine have been analyzed in terms of the supramolecular interaction of multiple phenyl embraces which are concerted supramolecular motifs maintained by phenyl-phenyl attractive interactions. The name phenyl embrace signifies the three attributes of:

(i) participation of two or more phenyl groups from each partner molecule;

(ii) geometrical concertedness;

(iii) strong attraction.

This is one strategy for recognizing concerted and elaborated supramolecular motifs to increase understanding of the bonding and potential chemical reactivity.

Dance and Scudder (1995, 1996a, 1997, 1998) have identified patterns of crystal packing, for a variety of compounds, which are constructed from multiple phenyl embraces. A multiple phenyl embrace (MPE) is a supramolecular motif comprised of a set of concerted phenyl-phenyl attractions. It is well established that the most favorable attractive interactions between pairs of phenyl rings are those involving the *ef* and offset-face-to-face (*off*) geometries. In the *ef* geometry (and the closely related vertex-to-face, *vf*, geometry) the two rings are inclined to each other and H atoms of one are directed towards the π-electron cloud of the other, while in the *off* geometry the two rings are approximately parallel and are positioned such that H atoms of one overlap the π-electron cloud of the other. The Coulombic H$\cdots\pi$ energy provides the directionality and offset in these cases. Perfectly eclipsed aromatic rings necessarily have a repulsive interaction as shown in Figure 2.3. The main component of attractive energy for this case is dispersion and the ring-to-ring contact distance is expected to be longer.

Six-fold Phenyl Embrace

The supramolecular structures of bis(triarylphosphine) compounds are usually dominated by six-fold phenyl embraces in which the three phenyl rings of an XPh_3 moiety are directed towards three phenyl rings from the XPh_3 partner moiety with the formation of six good intermolecular *ef* interactions (Dance & Scudder, 1995, 1996a). This sextuple phenyl embrace is ubiquitous in crystals containing Ph_4P^+ cations and in molecules with the frequently used PPh_3 terminal ligand: the phenyl groups of one Ph_4P^+ can engage in several multiple phenyl embraces. The six-fold phenyl embrace (6PE) comprised of a concerted cycle of six *ef* intermolecular motifs is illustrated in Figure 2.4 for Ph_4P^+ (hydrogen atoms omitted, the terminal phenyl rings are not involved here). Each arrow is from the edge of one ring to the face of another, across the intermolecular space. Each ring is the donor in one *ef* and the acceptor in another (Dance & Scudder, 1996b).

Dance and Scudder continued to develop the ideas of multiple phenyl embraces, finding a multitude of types. Several higher order motifs were found prompting reconsideration of the earlier abbreviations for multiple phenyl embraces. They replaced the adjectives quadruple and sextuple with arabic numerals, describing the multiple phenyl embraces as *n*-phenyl embraces. Thus, the orthogonal quadruple phenyl embrace (OQPE, Dance & Scudder, 1996a) became the O4PE (orthogonal 4-fold phenyl embrace), the parallel quadruple phenyl embrace (PQPE) became the P4PE (parallel 4-fold phenyl embrace), the sextuple phenyl embrace (SPE, Dance & Scudder, 1996a) became the 6PE, the zig-zag infinite sextuple phenyl embrace (ZZISPE, Dance & Scudder, 1996b) became ZZI6PE, and the hexagonal array of sextuple phenyl embraces (HASPE), became the HA6PE (Dance & Scudder, 1997).
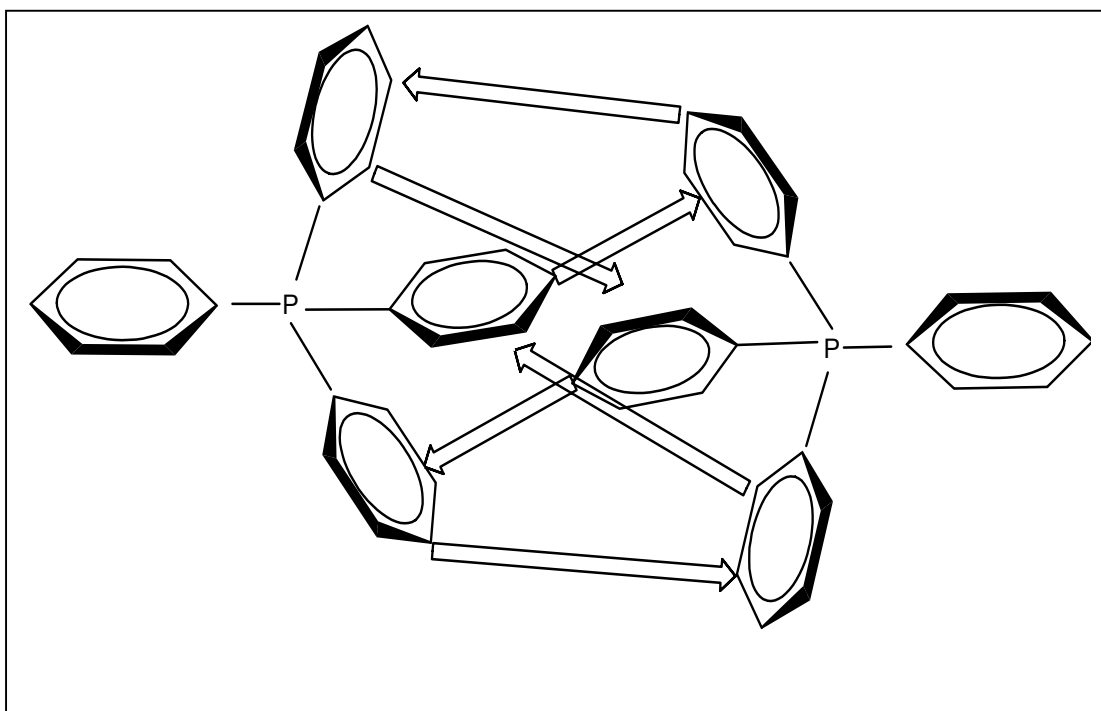
Figure 2.4. Representative sixfold phenyl embrace (6PE).

Fourfold Phenyl Embraces

There are other embrace motifs between Ph_4P^+ cations in which only two phenyl rings from each cation are used. These are called fourfold phenyl embraces, or 4PE. There are two types of 4PE. In the parallel 4PE (P4PE, illustrated in Figure 2.5) the C–P–C planes are approximately parallel with one *off* interaction across the center of the embrace and two *ef* interactions between the *off* related rings and the remaining two rings. In the orthogonal 4PE (O4PE, illustrated in Figure 2.6) the two C–P–C planes for the four phenyl rings are approximately orthogonal and there is a concerted cycle of four *ef* interactions between rings. The energy of an *off* interaction depends on the overlap, which determines the number and strength of the C−H···π interactions. Generally, an *off* interaction has greater energy than an *ef* interaction, but not twice as great, thus the P4PE interaction is slightly weaker than the O4PE interaction.
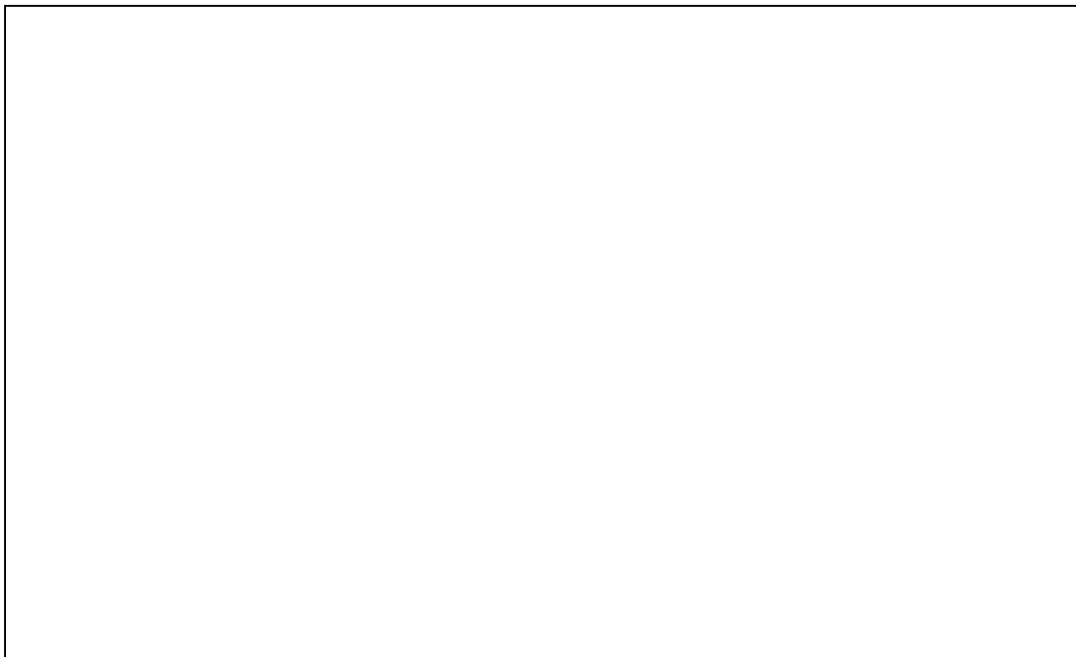
Figure 2.5. Representative parallel fourfold phenyl embrace (P4PE).
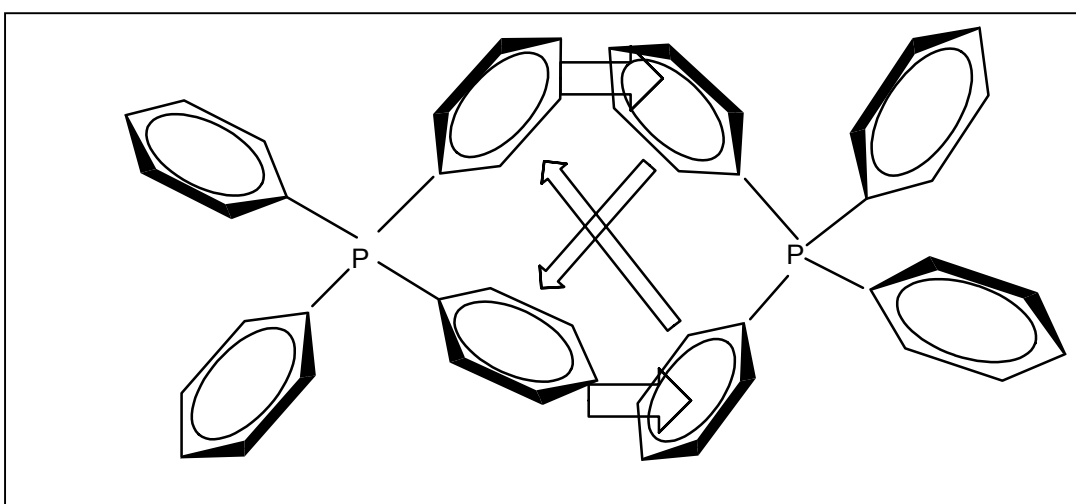
Figure 2.6. Representative orthogonal fourfold phenyl embrace (O4PE).

Larger multiple phenyl embraces, including the enlarged 6PE (E6PE), the hybrid 6PE (H6PE), and elaborate higher-order 8-fold phenyl embrace (with subtypes P8PE and O8PE) and 12-fold phenyl embrace, 12PE, have also been described (Dance & Scudder, 1998). Inclusion of aromatic solvent molecules in the lattice appears to favor the more elaborate motifs.

2.3 Crystallization

Crystallization is a separation and purification technique employed to produce a wide variety of materials. Crystallization from a solution may be defined as a phase change in which a crystalline product is obtained from a solution. A solution is a mixture of two or more species that form a homogenous single phase. Solutions are normally thought of in terms of liquids, however, solutions may include solid suspensions. Typically, the term solution has come to mean a liquid solution consisting of a solvent, which is a liquid, and a solute, which is a solid, at the conditions of interest. The crystallization process can be divided into three elementary steps: achievement of supersaturation, nucleation, and crystal growth (Ohtaki, 1998).

Achievement of Supersaturation

A solution is said to be saturated when it is in equilibrium with the solid phase. The concentration of such a saturated solution depends on temperature, and generally increases with temperature. A solution in which the solute concentration exceeds the equilibrium solute concentration at a given temperature is known as a supersaturated solution. There are five main methods to generate supersaturation, namely the following:

(i) Temperature change (mainly cooling);

(ii) Evaporation of solvent;

(iii) Chemical reaction;

(iv) Changing the solvent composition (*e.g.* solvent diffusion experiments);

(v) Changing the solute composition (*e.g.* salting out)

The Ostwald-Miers diagram shown in Figure 2.7 illustrates the basis of all methods of crystal growth from solution. The solid line represents a section of the curve for the solute/solvent system. The upper dashed line is referred to as the super-solubility line and denotes the temperatures and concentrations where spontaneous nucleation occurs (Mullin, 2001).
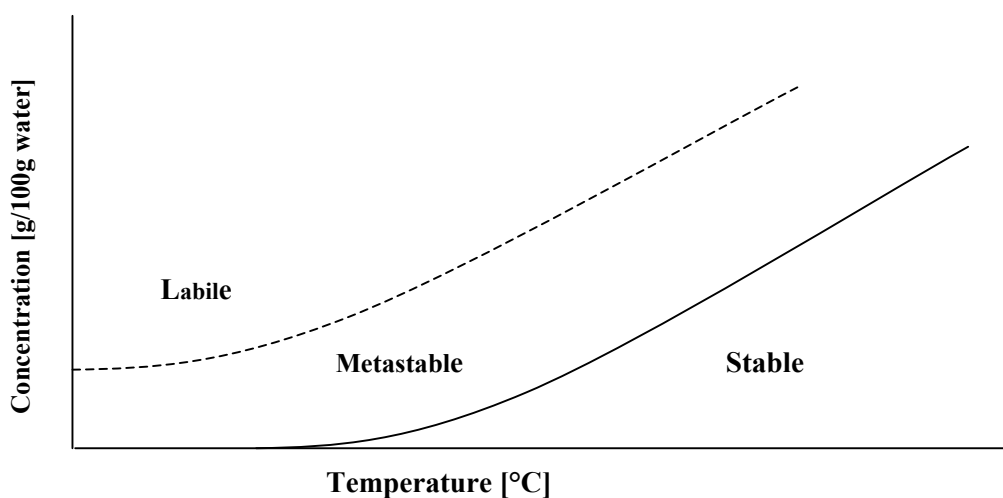
Figure 2.7. Oswald-Miers diagram for a solute/solvent system.

Nucleation

Primary nucleation from a supersaturated solution can be divided into homogeneous and heterogeneous nucleation. The former occurs spontaneously, while the latter is induced by impurities or foreign particles present in the solution. Heterogeneous nucleation might be suppressed by filtration of the solution. Secondary nucleation is induced by crystals and is connected to the process of seeding. During the induction period, different kinds of embryos form by chemical aggregation of precursor species, any of which may or may not disintegrate. As a result of such fluctuations, an embryo will grow in time, and eventually reach the

critical size at which crystal growth can occur spontaneously. When an embryo reaches this critical size it is called a nuclei. Different types of embryos may result in different types of nuclei (and by extension different types of crystal). The rate of nucleation can be derived from crystal size distribution measurement of the final crystallization product, and size increment measurements of the large crystals during the crystallization process, followed by extrapolation of the size vs. time curve to zero time. As nucleation and crystal growth are assumed to consume the same precursor species, the nucleation rate is expected to go through a maximum and decline again after a certain period when the consumption of precursor species by crystal growth limits the formation of new nuclei (Kashchiev, 2000).

Crystal Growth

After nucleation occurs, crystal growth can start. The nuclei will grow by integration of precursor species towards full-grown crystals. Experimental crystallization curves, giving the yield of crystalline material in time, usually exhibit an S-shape profile. The inflection points of these curves separate the period of autocatalytic increase of crystalline mass from the stage of delayed crystal growth. The autocatalytic nature of the first stage of the crystallization reflects the self accelerating behavior of a crystallization process. Presently, it is believed that the crystal growth occurs at the crystal plane-solution interface by the condensation of dissolved secondary units onto the growing crystal plane followed by surface migration, reorientation, loss of excess molecules of solvation, and any other changes required for incorporation of the growth unit into the crystal. In general, temperature and time have a positive influence on the crystal formation process. Raising

temperature will increase both the nucleation rate and the growth rate. The crystallinity of the samples normally increases in time (Markov, 2003).

2.4 Characterization Techniques

Infrared Spectroscopy (IR)

The infrared region of the electromagnetic spectrum lies between the visible and microwave regions. By convention, the infrared region is frequently divided into three sections:

Region	Wavenumber Range (cm^{-1})	Wavelength Range (μm)
Near-infrared	14,000-4,000	0.75-2.5
Mid-infrared	4,000-400	2.5-25
Far-infrared	400-10	25-1,000

The mid-infrared, or fundamental vibration region, is the most useful area of the spectrum for analytical spectroscopy.

Infrared spectroscopy theory states that a molecule may absorb infrared radiation of the appropriate frequency to excite it from one vibration or rotational level to another. When a beam of infrared energy, covering a broad frequency range, passes through a sample, the energy at certain frequencies is absorbed by the sample. A graph of energy absorbed vs. frequency is the absorption spectrum of the sample. The spectrum is characteristic of the particular molecule and its molecular motions (Gunzler & Gremlich, 2002).

Fourier transform infrared (FTIR) spectroscopy measures vibrations of functional groups and highly polar bonds. Thus, these chemical fingerprints are made

29

up of the vibrational features of all the components. An FTIR spectrometer records the interaction of IR radiation with experimental samples, measuring in the time domain and transforming the time domain spectrum to the frequency domain spectrum to give where the sample absorbs the radiation and the intensities of the absorptions. Determining these frequencies allows identification of the sample's chemical makeup, since chemical functional groups are known to absorb light within specific ranges of frequencies (Griffiths & de Haseth, 1986).

The Infrared Spectrometer

The main component of an FTIR spectrometer is the Michelson interferometer, as illustrated in the Figure 2.8.
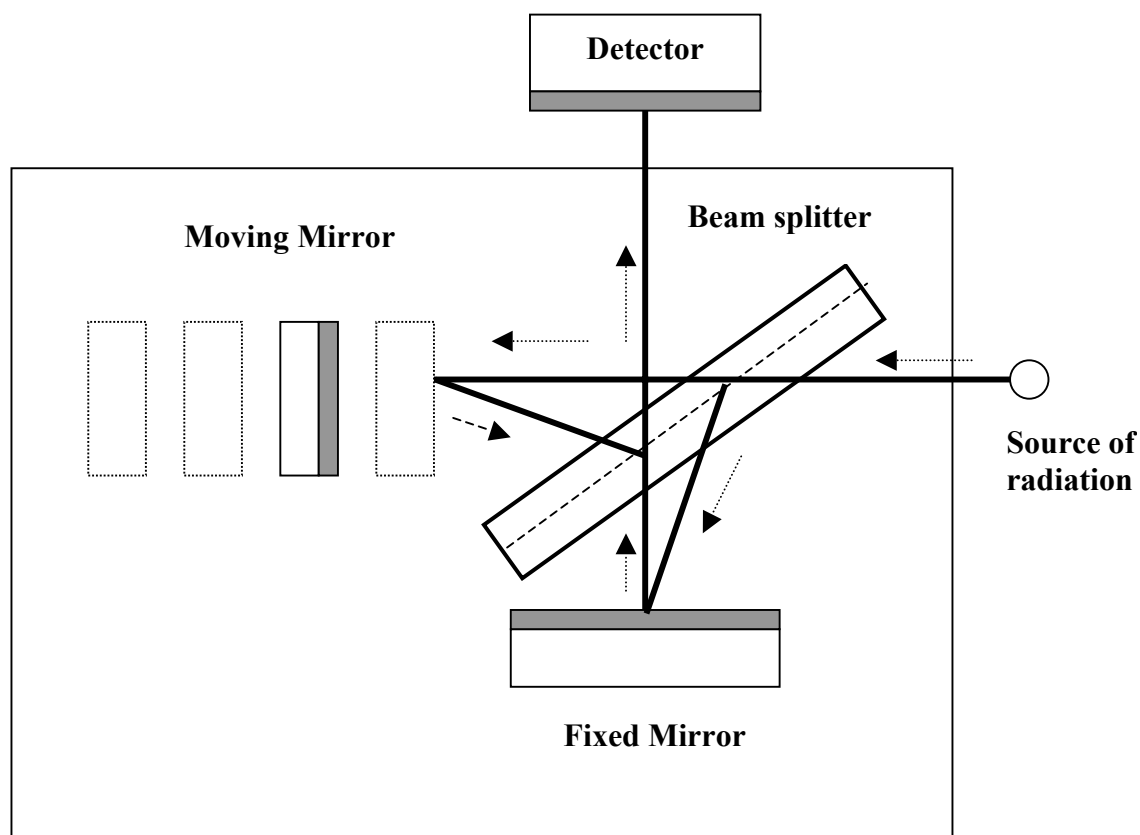
Figure 2.8. Schematic diagram of the Michelson interferometer.

The interferometer contains a fixed mirror, a movable mirror, and a beam splitter. The beam splitter transmits half of the incident radiation to the moving mirror and reflects the other half to the fixed mirror. The two beams are reflected by these mirrors back to the beam splitter where they recombine. When one mirror, the moving mirror is equidistant from the beam splitter, the amplitudes of all frequencies are in phase and recombine constructively. This position of zero path difference, or zero retardation, is where the interferogram center-burst occurs. As the moving mirror is moved away from the beam splitter (retarded), an optical path difference is generated. As the position of the moving mirror changes, the two beams travel different distances within the interferometer before recombining. A pattern of constructive and destructive interference is generated based on the position of the moving mirror and the frequency of the retardation. Thus, the intensity of the radiation varies in a complicated pattern, as a function of mirror movement, and the output beam is the result of modulation by the interferometer. This modulated output beam is then directed through the sample compartment to the detector. At the detector it generates a continuous electrical signal called an interferogram (Skoog & Leary, 1992, pp 113-120).

The moving mirror is driven at a constant velocity by a linear motor under computer control to vary the optical path difference. A beam from a He-Ne laser, operating at 632.8 nanometers, is also passed through the interferometer to its own detector, where it generates a references signal which enables the spectrometer electronics to sample the interferogram at precise intervals. The computer converts the interferogram into a single-beam spectrum by a Fourier transform (Skoog & Leary, 1992, pp 266-270).

The single-beam background spectrum is the spectrum of the source modified by the transmission characteristics of the beam splitter and the response characteristics of the detector. Most grating instruments (dispersive) are double beam spectrometers which measure the spectrum of the radiation that passes through the sample and automatically ratio it to the spectrum of the source. This results in a transmission spectrum directly. However, FTIR instruments first collect the spectrum of the source (single-beam background spectrum) and store it on disk. Then the sample is inserted in the instrument and the single-beam spectrum of the source, modified by the absorption due to the sample is collected and ratioed against the single-beam background spectrum to obtain the desired transmission spectrum (Ferraro & Krishhmann, 1990).

In this study FTIR was used to characterize the $Ni(N_3)(NO)(PPh_3)_2$ complex. Because the complex contains nitrosyl, and azido ligands which have very intense bands in relatively clean spectral regions, the position of nitrosyl and azido bands can confirm the presence of ligands. Examples of IR bands in azido complexes are listed in Table 2.3.

In this work the FTIR characterization was done on solid phase material. Powders are generally prepared by grinding with potassium bromide (KBr) powder and then pressed into a disk. The method of preparation of a powder sample is generally determined by the information required or the chemical/physical stability of the sample. KBr does not contain bands in the mid-IR region of the spectrum, and therefore preparation as KBr disks potentially loses less information. Samples dispersed in KBr powder must be homogenously dispered, with a particle size small

Table 2.3. IR Bands of Some Azido Complexes.

Complexes	IR Bands, cm^{-1}	Reference
[Ti(NMe$_2$)$_2$(N$_3$)$_2$bipy]	ν_{NNN}- 2079.52 (s,sh)	Carmalt, C. J., *et al*., 1997.
[Ti(NMe$_2$)$_2$(N$_3$)(py)$_2$]	ν_{NNN}- 2075.12 (s,sh)	Carmalt, C. J., *et al*., 1997.
[(*n*-Pr)$_2$ATI]SnN$_3$, molecule 2	ν_{NNN}- 2039 (s,sh)	Ayers, A. E., *et al*., 2000.
[Cu(trpn)(N$_3$)]ClO$_4$	ν_{NNN}- 2045 (s,sh)	Massoud, S. S., *et al*., 1999.

enough not to cause scatter (theorectically < 2 microns). The strength of an IR absorption spectrum is dependant on the number of molecules in the beam. With a KBr disk the strength will be dependent on the amount and homogeneity of the sample dispersed in the KBr powder. The optimum amounts of sample and KBr may vary with the bulk density of the sample or other diluents and will have to be varied according to the diameter of the disk required.

X-ray Diffraction

X-rays are an electromagnetic radiation of wavelength about 1 Å (10^{-10} m), which is about the same size as atomic distances in solids. Thus, it can be used to probe the crystalline structure at the atomic level. X-ray diffraction has been used in two main areas, for the fingerprint characterization of crystalline materials and the determination of their structures. Each crystalline solid has its unique characteristic X-ray pattern which may be used as a "fingerprint" for its identification. X-ray crystallography may be used to determine the structure of a single crystal species, *i.e.* how the atoms pack together in the crystalline state and what the interatomic distances and angles are. These unique properties make X-ray diffraction one of the

most important characterization tools used in solid state chemistry and material science.

An important equation for X-ray diffraction is the Bragg equation:

$$n\lambda = 2d\sin\theta$$

where, n is an integer, λ is the wavelength of the radiation, d is the perpendicular spacing between adjacent planes in the crystal lattice, and 2θ is the angle between the incident and the reflected X-ray beams.

Figure 2.9 shows X-rays "reflected" from planes in the crystal lattice. Electromagnetic waves 1 and 2 penetrate the parallel planes P1 and P2 at points A and B making the angle θ. The generated waves 1´ and 2´ are the reflected beams. The angle θ of the incident and reflected beams must be equal relative to the incoming and outgoing beams and the normal to the reflecting planes themselves all of which lie in one plane. Constructive interference (in-phase) of the waves emanating from points A and B occurs only when the path lengths traveled are an integral multiple of the wavelength, $n\lambda$. It is seen that the path-length difference is $2d\sin\theta$. When this equals $n\lambda$, the Bragg equation is satisfied, and constructive interference results producing a diffraction maximum or "reflection".

When considering diffraction of X-rays from lattice planes in a unit cell, the planes must be designated in a consistent manner. This is done by assigning Miller indices to the lattice planes. Miller indices are ordered integer triples, (*hkl*), where the
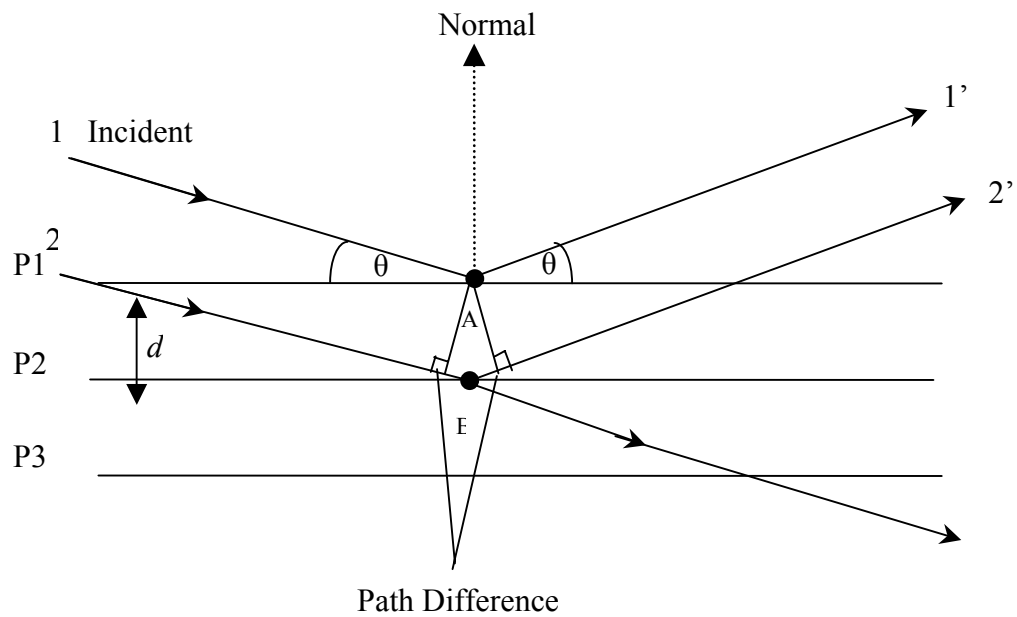
Figure 2.9. Reflection of X-rays from crystal lattice planes.

also used to designate lattice points *hkl* that correspond to the (*hkl*) family of planes.

Each "reflection" of an X-ray beam from a crystal is assigned unique *hkl* values.

Miller indices representing lattice planes and lattice points are shown in Figure 2.9(a)

and (b), respectively (Drago, 1992, pp 689-691).
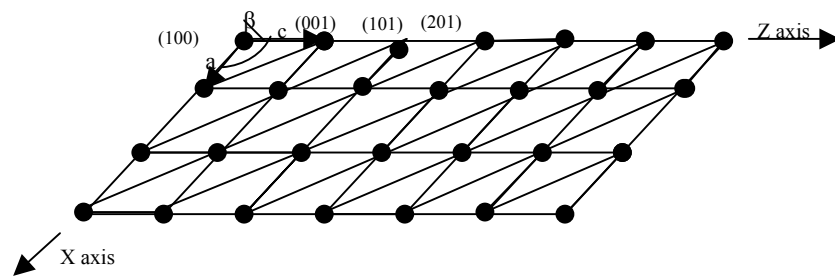
(a) Direct Lattice
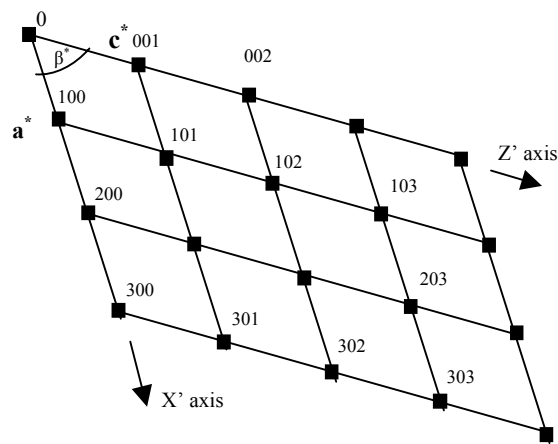
(b) Reciprocal Lattice

Figure 2.10. Direct and reciprocal lattices.

CHAPTER III

EXPERIMENTAL

3.1 Materials and Equipment

Chemicals and Materials

1. Nickel(II) bromide trihydrate (NiBr$_2$·3H$_2$O); Fluka reagent, 98%, Mr 272.55, CAS-No. 7789-49-3.

2. Sodium azide (NaN$_3$); Sigma reagent, 99.5%, M$_r$ 65.01, CAS-No. 26628-22-8.

3. Triphenylphosphine (PPh$_3$); Fluka, ~99% (HPLC), M$_r$ 262.30, CAS-No. 603-35-0.

4. Sodium nitrite (NaNO$_2$); M$_r$ 69.00, CAS-No. 7632-00-0.

5. Ethyl alcohol, absolute (CH$_3$CH$_2$OH); Carlo Erba reagent RPE, (v/v) 99.8%, M$_r$ 46.070, CAS-No. 64-17-5.

6. Hexane (CH$_3$(CH$_2$)$_4$CH$_3$); Carlo Erba reagent RPE, 99% (GLC), M$_r$ 86.173, CAS- No. 110-54-3.

7. Methanol (CH$_3$OH); Carlo Erba reagent RPE, 99%, M$_r$ 32.042, CAS-No. 67-56-1.

8. 2-Propanol (CH$_3$CH(OH)CH$_3$); Merck, gradient grade for liquid chromatograph, M$_r$ 60.10, CAS-No. 67-63-0.

9. Tetrahydrofuran (THF, C$_4$H$_8$O); Mallinckrodt chrom AR HPLC, M$_r$ 72.11, CAS-No. 109-99-9.

10. High vacuum grease.

11. Molecular Sieve No. 4A; Union Carbide Company.

12. Molecular Sieve No. 5A; Union Carbide Company.

13. Nitrogen; H.P. grade 99.95%; TIG company, CAS-No. 7727-37-9.

Methanol was dried by storing over No. 4A Molecular Sieve, and all other solvents were dried by storing over No. 5A Molecular Sieve, prior to use.

Glassware and Apparatus

1. Round bottom flask, 250 mL with two necks

2. Schlenk tubes

3. Double-manifold vacuum line

4. Solids container

5. Hot plate and magnetic stirrer

6. Syringe with needle

7. Condenser

8. Thermometer

9. Desiccators

10. Mortar and pestle

3.2 Instrumentation

Fourier Transform Infrared Spectroscopy (FTIR)

A Bio-Rad FTS 175C Fourier transform infrared spectrophotometer was used to record the mid-IR spectra of samples (4000-400 cm^{-1}). Approximately 0.5 mg of sample was mixed with 300 mg of KBr powder, dried at 120°C for 1 hour before use, and ground to a very fine powder with an agate mortar and pestle. The ground powder was pressed into a 16 mm transparent disk using a hydraulic press with an equivalent weight of about 10 tons for 1 minute. The spectra were obtained as an average of 16 scans with 1 cm^{-1} resolution.

Single Crystal X-ray Diffraction

Data were collected at 298 K on a Bruker-Nonius KappaCCD area detector diffractometer**.** The diffractometer was equipped with a highly-oriented pyrolytic graphite crystal incident beam monochromator and a molybdenum $K\alpha$ ($\overline{\lambda}$ = 0.71073 Å) x-radiation source operated at tube power levels of 50 kV and 20 mA. The X-ray beam was conditioned with an *ifg* focusing optics incident beam collimator which increases the X-ray intensity at the sample by approximately 50-80% for molybdenum $K\alpha$ radiation.

3.3 Syntheses

The syntheses of nitrosyl containing complexes were carried out under a nitrogen atmosphere. All solvents and starting materials were purged with nitrogen prior to use (Shriver & Drezdzon, 1986). Apparatus set up for the synthesis is shown in Figure 3.1.
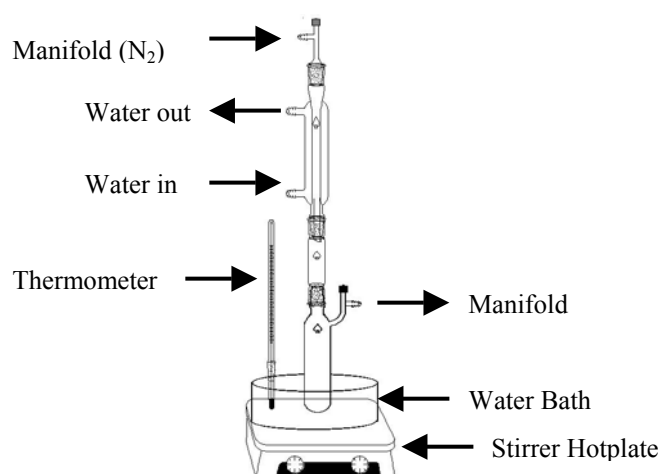
Figure 3.1. Refluxing under a nitrogen atmosphere.

Synthesis of Dibromobis(triphenylphosphine)nickel(II) (Venanzi, 1958)

$$\text{NiBr}_2 \cdot 3\text{H}_2\text{O} + 2\text{PPh}_3 \xrightarrow{\text{2-propanol}} \text{NiBr}_2(\text{PPh}_3)_2 \downarrow + 3\text{H}_2\text{O}$$
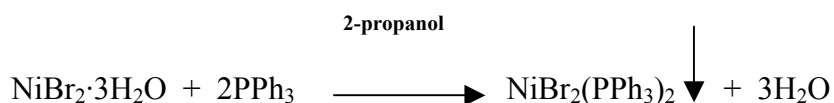
Nickel bromide trihydrate (5.45 g, 20 mmol), was dissolved with 100 mL of boiling 2-propanol in a 250 mL Erlenmeyer flask, and triphenylphosphine (10.49 g, 40 mmol), was dissolved in 100 mL boiling 2-propanol in a 150 mL Erlenmeyer flask. The triphenylphosphine solution was added into the nickel bromide solution. The olive-green microcrystalline precipitate, when kept in contact with its mother-liquor for 24 hr, gave dark green crystals which were filtered off using a Buchner funnel. Crude yield of dark green $\text{NiBr}_2(\text{PPh}_3)_2$ 13.10 g, 18 mmol (88.16%). Physical characterization data is given in Table 3.1.

Table 3.1. Physical Characterization of $\text{NiBr}_2(\text{PPh}_3)_2$ and $\text{NiX(NO)(PPh}_3)_2$. ($\text{X} = \text{Br}^-, \text{N}_3^-$).

Complexes	Crude Yield (%)	Color	Melting Point (°C)	Infrared Frequencies (cm^{-1})		
				ν_{NO}	ν_{NNN}-	ν_{NiP}
$\text{NiBr}_2(\text{PPh}_3)_2$	88.16	green	222-225			418(w)
$\text{NiBr(NO)(PPh}_3)_2$	78.58	dark blue	200-205	1715(s)		419(m)
$\text{Ni(N}_3)(\text{NO)(PPh}_3)_2$	48.99	deep blue-black	190-193	1715(s)	2050(s)	419(w)

s = strong, m = medium, w = weak.

Synthesis of Bromonitrosylbis(triphenylphosphine)nickel (Feltham, 1964)

$$NiBr_2(PPh_3)_2 + NaNO_2 + PPh_3 \xrightarrow{\text{THF}} NiBr(NO)(PPh_3)_2 + NaBr\downarrow + OPPh_3\downarrow$$
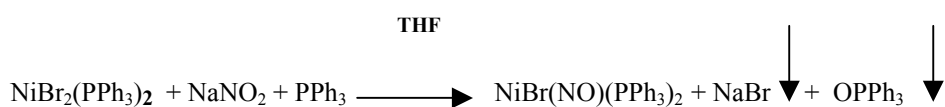
A mixture of $NiBr_2(PPh_3)_2$ (5.00 g, 6.73 mmol), as prepared above and PPh_3 (1.77 g, 6.75 mmol), were dissolved in 50 mL of THF. Freshly ground $NaNO_2$ (7.94 g, 115 mmol), dried under vacuum over molecular sieve 5A, was added along with seven glass beads to a standard Schlenk apparatus connected to a double manifold vacuum/nitrogen line. The solution was refluxed under a nitrogen atmosphere for 40 min on a water bath, cooled, filtered, and concentrated to 35 mL. Addition of 25 mL of hexane gave a dark blue oil which was separated and treated with 50 mL of cold methanol to induce crystallization. The dark blue $NiBr(NO)(PPh_3)_2$ crystals were separated and dried; 3.67 g, 5.29 mmol, (78.58% crude yield). Physical characterization data is given in Table 3.1.

Synthesis of Azidonitrosylbis(triphenylphosphine)nickel(II) (Enemark, 1971)

$$NiBr(NO)(PPh_3)_2 + NaN_3 \xrightarrow{\text{MeOH}} Ni(N_3)(NO(PPh_3)_2 + NaBr\downarrow$$
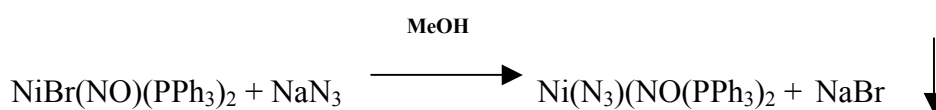
$NiBr(NO)(PPh_3)_2$ (1.04 g, 1.5 mmol) and NaN_3 (0.20 g, 3 mmol) were dissolved in dry methanol 10 mL and the solution was refluxed for 1 hour (dark blue solution and deep blue black precipitate), then allowed to stand at room temperature under inert gas 2 days and filtered to give a deep blue-black precipitate. The product was dried by an inert gas purge, 0.48 g, 0.73 mmol, (48.99% crude yield). Physical characterization data is given in Table 3.1.

3.4 Recrystallization

Azidonitrosylbis(triphenylphosphine)nickel(II) was recrystallized using the vapor diffusion technique under an inert atmosphere. Deep blue-black precipitate, 0.1 g, from the synthesis was dissolved in a quantity of hot benzene that would make a saturated solution at room temperature. The hot solution was filtered to remove solid impurities. The filtrate was placed in a small tube which was placed inside a Schlenk tube. Hexane (nonsolvent) was placed in the Schlenk tube, which was purged with nitrogen to establish an inert atmosphere. The stopcock was closed to maintain the nitrogen/solvents atmosphere over the solution, and the apparatus was set in a quiet place at room temperature. Slow diffusion of nonsolvent into the solution and solvent out of the solution caused crystals to form inside the small tube. Elemental analysis data for the recrystallized product is given in Table 3.2 Bromine analysis was not done.

Table 3.2. Elemental Analysis Data for $NiN_3(NO)(PPh_3)$.

Element	Ni(%)	C(%)	H(%)	P(%)	O(%)	N(%)
Calcd.($NiN_3(NO)(PPh_3)$)	9.0	66.1	4.6	9.4	2.4	8.5
Calcd.(Br disorder)	7.9	58.4	4.1	8.4	2.2	7.6
Found	9.2	66.3	4.6	9.4	2.3	7.7

3.5 Analysis of Crystal Structure

Methodology

The supramolecular structure interactions were identified by a combination of distance and angle calculations along with examination of graphical images of molecules and fragments of molecules. Inter- and intra-molecular contact distances

were calculated with the ORTEP-III program (Burnett & Johnson, 1996). Analysis

was begun by calculating Ni−P···P′−Ni′ colinearity angles and P···P' separations in

the range 5.5-8.0 Å identified by Dance and Scudder (1995) for concerted phenyl

embraces. The colinearity parameter is defined as half the sum of M−P···P′ (α) and

P···P′−M′ (β) angle ($\alpha+\beta$)/2 (α and β are illustrated in Figure 3.2). The criteria for

the calculation to ensure that all meaningful P···P separation interactions of

$Ni(X)(NO)(PPh_3)_2$ were examined was to consider all the near P···P distances around

P1 and P2 from one molecule (position 55501 in the language of Atom Designator

Codes used by ORTEP as explained in Appendix A) to P1 and P2 of all neighboring

molecules with symbol NNTTTSS (as described in Appendix A) where SS included

all symmetry operations of space group $P2_1/c$ and TTT included unit translations

from −2 to +2 for each axis (thus calculation of all P···P distances from the origin P to

all the phosphorus positions in the 125 unit cells in the neighborhood. For the

purposes of this thesis the maximum P···P distance retained was 12 Å. Since the

colinearity angle is required the calculations were initiated by a 102 instruction to

ORTEP which gives both interatomic distances and interatomic angles about each

origin atom (see Appendix A for a description of the 102 instruction).
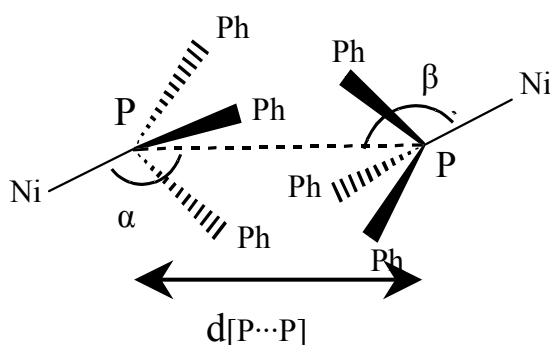
Figure 3.2. Colinearity parameter in sixfold phenyl embraces.

The crystal data are interpreted from an ORTEP instruction file and the results of the calculations are given in an output file from the program. The results include the coordinates of the origin and target phosphorus and nickel atoms within the 12 Å distance criteria specified, the P⋯P distances, the M−P⋯P′ and P⋯P′−M′ angles, and the atom designator codes for all atoms involved in each P⋯P interaction. The coordinates of the midpoint of each P⋯P interaction and the colinearity angle for each interaction were calculated from the ORTEP results and are listed in Appendix B, Table B.5. The coordinates of the P⋯P midpoints were added to the ORTEP input file to aid in drawings in order to consider additional interactions between the phenyl rings on interacting pairs of PPh$_3$ ligands related to each other through some type of phenyl embrace.

Sixfold phenyl embraces (6PE) are characterized by intermolecular d[P⋯P] < 8 Å and ∠[M−P⋯P′−M′] colinearity in the range 160-180° (Dance & Scudder, 1995), and fourfold phenyl embraces (4PE) by d[P⋯P] ≤ 9 Å (Dance & Scudder, 1996b).

When calculating contact distances between carbon atoms of the phenyl rings of one molecule (55501) to hydrogen atoms of the phenyl rings of another molecule (NNTTTSS) or from hydrogen atoms of phenyl rings of one molecule to the carbon atoms of the phenyl rings of another molecule, a maximum cutoff distance of 3.4 Å was used. Only distances were required, so a 101 instruction was input into ORTEP.

Additional potential intermolecular contacts were identified by calculating contact distances from the phenyl carbon atoms to the idealized hydrogen atom positions (*ef* contacts), to the phenyl carbon atoms (*ff* contacts), and to the hydrogen bond acceptors for other nonbonded contacts. Ring C⋯H contact distances less than 3.6 Å were examined graphically to determine if they were *ff* contacts. Remaining

ring C⋯H contact distances less than 3.2 Å were examined to determine if they were *ef* contacts or van der Waals edge-to-edge, *ee*, contacts.

Interactions between adjacent phenyl rings are indicated as *ef*, van der Waals *ee* or *ff* interactions based on the calculated distances and the relative positions of the two rings. The relative positions of the rings involved in a given separation were analyzed graphically, generally by drawing the contents of a sphere in direct space with an appropriate radius about the P⋯P midpoint, or centered on the hydrogen atom of the interaction. The sphere was drawn projected on one of the interacting phenyl rings and then drawn perpendicular to the same interacting phenyl ring. Sometimes it was useful to draw the same two views of the second ring as well. From the directionality of each phenyl ring interaction, the type of π stacking can be determined; if the phenyl rings overlap and are perpendicular to each other it is an *ef* interaction, if the phenyl rings overlap and are parallel to each other it is an *off* π stacking, or if the rings do not overlap but only touch on the edges it is a van der Waals contact or dispersion interaction. Finally, counting the number of concerted interactions gives the order of the phenyl-phenyl embrace.

The two phenyl rings in each *ef* contact are inclined to each other and one or two H atoms of one ring are directed towards the π electron cloud of the other. The two phenyl rings in each *ee* van der Waals contact have H atoms of one ring directed towards H atoms of the second ring. C⋯H contact distances in the appropriate range for *ee* interactions, 2.8 to 3.2 Å (Dance & Scudder, 1995) were examined carefully to distinguish between *ef* and *ee* character.

For an *off* contact two rings must be approximately parallel and positioned such that H atoms of one are close to the π electron density of the other (and vice

verse). Contact regions up to 3.6 Å (the normal $\pi\cdots\pi$ contact distance is 3.4 Å) were examined graphically to verify that the rings were in the appropriate relationship.

If the three phenyl rings of a PPh$_3$ group of one molecule interact to the three phenyl rings of a PPh$_3$ group on an adjacent molecule resulting in three *ef* and three face-to-edge interactions, the concerted multiple phenyl embrace is a sixfold phenyl embrace, 6PE. In the most common motif the six phenyl groups of two adjacent triphenylphosphine ligands can arrange such that there are six concerted *ef* interactions alternating from ligand A to ligand B, B to A, A to B, *etc*. The concerted 6PE thus formed will often be the strongest intermolecular interaction in a molecular crystal. Sextuple phenyl embraces result when the phenyl rings of two triphenylphosphine ligands are arranged in interlocking C$_3$ propeller configurations, usually related by an inversion center. An individual *ff* or *ef* interaction is only a few kJ mol^{-1}, but when concerted, the cooperative result can easily reach 33 to 46 kJ mol^{-1} (Scudder & Dance, 1998).

Fourfold phenyl embraces (4PE) involve two phenyl groups on each partner, with two geometrical subclasses depending on whether the C$_{ipso}$PC$_{ipso}$ planes on each molecule are approximately parallel (P4PE) or approximately orthogonal (O4PE).

The second part the supramolecular structure interaction is concerted NO and X (monoanion) to phenyl ring. These were calculated by 102 instructions input into the ORTEP program, and considering phenyl ring to NO and X contacts less than the sum of the respective van der Waals radii of C−H$\cdots$O (2.70 Å), C−H$\cdots$N (2.75 Å), C−H$\cdots$Cl (2.95 Å), C−H$\cdots$S (3.00 Å). Tabulations of van der Waals radii are given in Table 3.3. Bondi (1964) values were used in this study.

Table 3.3. van der Waals Radii.

Elements	Pauling, 1948 (Å)	Bondi, 1964 (Å)	Taylor & Kennard, 1982 (Å)
H	1.2	1.20	1.09
C		1.70	1.75
N	1.5	1.55	1.61
O	1.4	1.52	1.56
Cl	1.80	1.75	1.74
Br	1.95	1.85	1.85
S	1.85	1.80	1.79

CHAPTER IV[A]

SUPRAMOLECULAR INTERACTIONS IN AZIDONITROSYLBIS(TRIPHENYLPHOSPHINE)NICKEL

4.1 Abstract

Azidonitrosylbis(triphenylphosphine)nickel was synthesized from NiBr(NO)(PPh$_3$)$_2$ by a metathesis reaction with excess NaN$_3$. The structure has been redetermined based on an X-ray data set collected on a KappaCCD diffractometer to improve the model for the azide region. The deep blue-black compound crystallizes in the monoclinic space group P2$_1$/c with unit cell parameters at 298 K of a = 13.597(5) Å, b = 19.098(8) Å, c = 12.562(4) Å, β = 98.59(5)°, V = 3221.89 Å^3, and Z = 4. The discrete pseudo tetrahedral molecules are interconnected into a three-dimensional supramolecular structure by concerted C−H···N, C−H···O, and C−H···π hydrogen bonds to the lone pair and π electron density of the azido, nitrosyl, and phenyl groups.

4.2 Introduction

Supramolecular synthons are made up of spatial arrangements of potential intermolecular interactions and play the same focusing role in supramolecular synthesis that conventional synthons do in molecular synthesis. One common synthon is the phenyl ring which can engage in offset-face-to-face (*off*) stacking interactions, placing the π systems of the aromatic rings in contact, or in edge-to-face (*ef*) interac-

_____

a. Published, Khosavithitkul & Haller, 2003.

tion between the phenylene hydrogen atoms of one ring and the π system of another.

Although an individual *off* or *ef* interaction involves only a few kJ mol^{-1} of energy, more complex synthons allow multiple interactions to occur in concert. A common such motif is the six phenyl groups of two adjacent triphenylphosphine ligands arranged in interlocking C3 propeller configurations, such that there are six concerted *ef* interactions alternating from ligand A to ligand B, B to A, A to B, *etc*. The concerted sixfold phenyl embrace (6PE) thus formed is often the strongest intermolecular interaction in a molecular crystal (Dance & Scudder, 1995) and in fact when there are two or more triphenylphosphines in the same molecule, the crystal structure is often dominated by chains of 6PE linked molecules.

Four-coordinate diphosphine nickel complexes have been studied extensively because of the stereochemical flexibility of their molecular structures. Examples are plentiful for both square planar and tetrahedral geometries. A notable example is the dibromobis(diphenylbenzylphosphine)nickel(II) complex which crystallizes with both the tetrahedral and the square planar forms in the same lattice (Kilbourn & Powell, 1970). Intermediate geometries are also known. The distorted pseudo tetrahedral structure of the $Ni(N_3)(NO)(PPh_3)_2$. complex, reported by Enemark (1971), is typical ($\angle(P-Ni-P) = 120°$; $\angle((N_3)-Ni-NO) = 129°$; NiP_2-NiN_2 dihedral angle 84.1°) of the intermediate geometry of all three structurally characterized members of the $Ni(X)(NO)(PPh_3)_2$ family. The supramolecular structures of the chloro and isothiocyanato analogs contain the expected 6PE chains, but the azido complex does not (Kiatpichitpong, 2002).

4.3 Experimental

Materials and Techniques

All manipulations were carried out under an atmosphere of purified nitrogen using standard Schlenk techniques. Reagent grade solvents and chemicals were purchased from commercial sources and used without further purification, except that solvents were dried with molecular sieve prior to use. Glassware was oven-dried at 150°C overnight.

Preparations

Synthetic methods for preparing azidonitrosylbis(triphenylphosphine)nickel have been previously reported (Enemark, 1971, Venanzi, 1958, Feltham, 1964). Bromonitrosylbis(triphenylphosphine)nickel and sodium azide were dissolved in absolute methanol. The reaction suspension was refluxed under a nitrogen atmosphere for 1 hour on a water bath and cooled. The desired product was filtered, washed with cold absolute methanol, dried under a nitrogen atmosphere, and recrystallized by solvent diffusion of hexane into a benzene solution to give deep blue-black crystalline product. The infrared spectrum was recorded on a Bio-Rad model FTS175C FTIR spectrometer.

X-ray Crystallography Study

A single crystal fragment of the deep blue-black compound was selected and mounted to the end of a hollow glass fiber with cyanoacrylate glue. Reflection intensities were collected at 298 K on a Bruker-Nonius KappaCCD four-circle area-detector diffractometer using the COLLECT (Nonius BV, 1998) software. The

diffractrometer was equipped with a graphite monochromator, a 0.3 mm *ifg* capillary collimator, and a fine focus X-ray tube (Mo K_α radiation, $\bar{\lambda}$ = 0.71073 Å) operating at 50 kV and 20 mA. The frame images were reduced to intensity data using EvalCCD (Duisenberg, Kroon-Batenburg & Schreurs, 2003) and the structure solved by direct methods using SIR97 (Altomare, Burla, Camalli, Cascarano, Giacovazzo, Guagliardi, Moliterni, Polidori & Spagna, 1999). All the hydrogen atoms were easily located from a subsequent difference electron density map.

After preliminary refinement, the largest feature on the difference electron density map was a peak between the coordinated and second nitrogen atoms of the azide group. The position was included in the refinement as a minor component bromo ligand. The occupancies of the bromo and azido ligands were refined with the constraint that they sum to unity. The coordinated and second azido nitrogen atoms, and the bromine atom were assigned a common isotropic atomic displacement parameter due to their proximity. Phenylene hydrogen atoms were included as idealized, riding-model (d[C–H] = 0.93 Å) isotropic contributions with U_{iso} = 1.1U_{eq}[attached carbon]. In the final model all nonhydrogen atoms were given anisotropic atomic displacement parameters except the partial bromine atom and the two partial nitrogen atoms of the azide group that overlap the minor component bromine atom, which were treated as noted above. Least squares refinement, electron density calculations, and idealized geometric parameters for hydrogen atom positions were provided by SHELXL−97 (Sheldrick, 1997). At convergence the occupancy of the azido ligand was 0.836(3), indicating approximately 16% bromo impurity in the

data crystal. Crystal data and details of the data collection procedures and structure refinement are presented in Table 4.1.

Potential 6PE phenyl embraces were characterized by intermolecular $d[P\cdots P]$ < 8 Å and $\angle[M–P\cdots P–M]$, colinearity, in the range 160-180° (Dance & Scudder, 1995). Systematic examination of all inter- and intra-molecular noncovalent contact distances were calculated with the ORTEP-III program (Burnett & Johnson, 1996). and other supramolecular structure interactions were identified from intermolecular contacts with $d[P\cdots P]$ < 9 Å (Dance & Scudder, 1996b). All interactions were confirmed by examination of graphical images of molecules and fragments of molecules.

Additional potential intermolecular contacts were identified by calculating contact distances to the idealized hydrogen atom positions (*ef* contacts), to the phenyl carbon atoms (face-to-face contacts, *ff*), and to the hydrogen bond acceptors for other nonbonded contacts. Ring $C\cdots H$ contact distances less than 3.6 Å were examined graphically to determine if they were *ff* contacts. Remaining ring $C\cdots H$ contact distances less than 3.2 Å were examined to determine if they were *ef* contacts or van der Waals edge-to-edge contacts.

Table 4.1. Crystal Data, Data Collection, and Structure Refinement Details for $Ni(N_3)(NO)(PPh_3)_2$.

Crystal data

Structure formula	$Ni(N_3)(NO)(PPh_3)_2$
Chemical formula	$C36H_{30}N4OP2Ni$
Chemical formula weight	713.82
Crystal system and space group	monoclinic $P2_1$/c (No. 14)
Unit cell a (Å)	13.597(5)
b (Å)	19.098(8)
c (Å)	12.562(4)
β (°)	95.862(9)
V (Å^3)	3221.89
Z	4
D_{calc} (Mg m^{-3})	1.35
Temperature (K)	298(2)
Absorption coefficient, μ (cm^{-1})	0.891
F(000)	1367

Data collection

Diffractometer	Bruker-Nonius KappaCCD
Radiation type / Wavelength (Å)	Mo K_α / 0.71073
Generator settings (kV/mA)	40 / 25
Absorption correction:	multiscan (SORTAV; Blessing, 1995)
Measured reflections	26251
Theta range for data collection	3.21-27.50
R_{int}	0.0542
Range of *h, k, l*	$-11 \leq h \leq 16, -22 \leq k \leq 24, -17 \leq l \leq 15$

Refinement

Refinement on	F^2
No. of unique reflections	7174
No. of observed reflections ($F_o > 4\sigma F_o$)	5012
R indices ($F_o > 4\sigma F_o$)	$R_1 = 0.0479, wR_2 = 0.0934$
R indices (all data)	$R_1 = 0.0882, wR_2 = 0.1158$
goodness of fit	1.138
Number of variables	393

Table 4.1. (continued)

Weighting scheme	$w = 1/[\sigma^2 F_o^2 + (0.0355P)^2 + 2.61P]$ where $P = [\max(F_o^2, 0) + 2F_o^2]/3$
Refinement program	SHELXL97 (Sheldrick, 1997)
Drawing program	ORTEP−III v 1.076 (Farrugia, 1997; (Burnett & Johnson, 1996)

4.4 Results and discussion

The IR spectrum shows a strong band at 2050 cm^{-1} assigned to the asymmetric N_3 stretching vibration of the terminal azide group and another strong band at 1715 cm^{-1} assigned to the nitrosyl NO stretching vibration confirming its presence.

Molecular Structure of Ni(N₃)(NO)(PPh₃)₂

The Ni(N$_3$)(NO)(PPh$_3$)$_2$ structure consists of discrete molecules with pseudo tetrahedral coordination geometry about the Ni atom as shown in Figure 4.1.

The P−Ni−P angle is 120.90(3)°, the N_3−Ni−NO angle is 129.1(2)°, and the dihedral angle between the P−Ni−P and N_3−Ni−NO planes is 84.7(1)°. The distances of within the nitrosyl ligand are normal, Ni−NO = 1.693(3) Å, N4−O = 1.129(4) Å, and Ni−N4−O = 152.7(3)°. The azido ligand is nonlinearly coordinated to the Ni atom, Ni−N1−N2 = 126.6(3)°, Ni−N$_3$ = 2.008(5) Å, N1−N2 = 1.150(7) Å and N2−N3 = 1.158(5) Å, and asymmetrically related to the two phosphine ligands (see Figure 4.1).
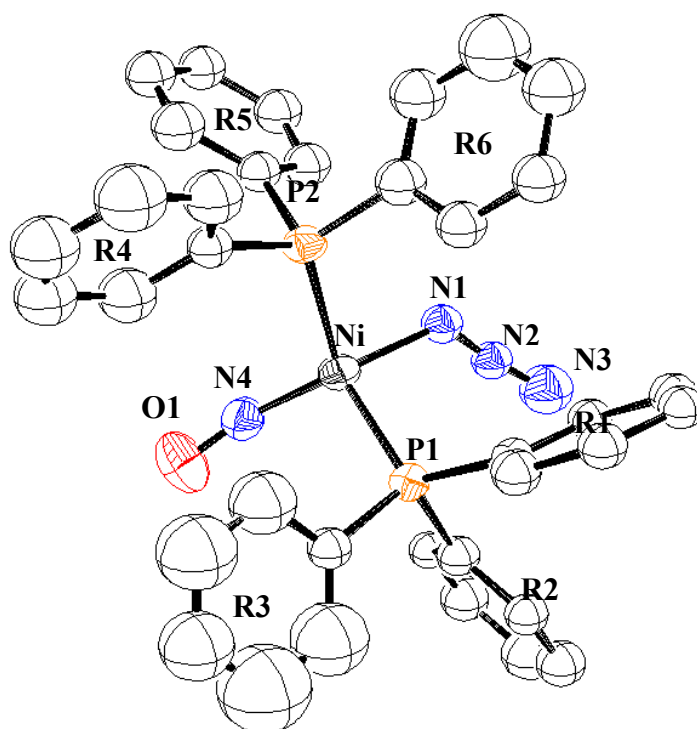
Figure 4.1. ORTEP perspective drawing of $Ni(N_3)(NO)(PPh_3)_2$. H atoms omitted for clarity.

An interesting feature previously noted for these four-coordinate nickel diphosphine complexes is the nonequivalence of the nominally, chemically equivalent Ni−P bonds, Ni−P1 = 2.2448(9) and Ni−P2 = 2.2891(8) Å, 50σ different. Kriege-Simondsen, Elbaze, Dartiguenave, Feltham, and Dartiguenave (1982) determined the structure of $Ni(NO)(NO_2)(PMe_3)_2$ at room temperature and at reduced temperature. They found that at room temperature the Ni−P distances were nonequivalent, but at reduced temperature they became equivalent. Therefore, they concluded that the nonequivalence is probably due to vibronic coupling.

Crystal Structure of $Ni(N_3)(NO)(PPh_3)_2$

The supramolecular structures of bis(triphenylphosphine) compounds are usually dominated by 6PE. The 6PE are easily found from intermolecular d[P···P] < 8

Å and [M−P···P−M], colinearities in the range 160-180° (Dance & Scudder, 1995). This is the case for both other known compounds in this series (Kiatpichitpong, 2002). The distance/colinearity parameters for the 6PE in the isothiocyanato complex are 7.087 Å/176.9° and 7.246 Å/173.0°, while those for the chloro complex are 7.163 Å/174.2°. Although the current structure has d[P···P] of 7.350 and 7.783 Å, the colinearities are 86.98 and 117.80°, and there are no 6PE in this structure.

One potential explanation for the lack of 6PE can be found in *intra*molecular noncovalent bonding. The strongest noncovalent interaction in the structure is a 2.493 Å intramolecular C−H···N interactions to the azido ligand lone pair on the nitrogen atom bonded to nickel. The phenyl ring involved in this interaction is rotated to lie approximately parallel to the Ni−P vector, thereby destroying the ideal geometry required to form a 6PE. Another strong *intra*molecular C−H···N interaction to the azido ligand π cloud involves the other triphenylphosphine ligand and disrupts the second possibility to form a 6PE. Thus, Kiatpichitpong (2002) suggested that the azido ligand, as the strongest hydrogen bond acceptor, may become the most important determiner of the supramolecular structure.

Another possible explanation comes from systematic examination of all intra- and intermolecular noncovalent contact distances, which led to identification of only two regions with highly concerted interactions. These regions alternate in the [001] direction as shown in Figure 4.2 to connect the molecules together into one dimensional chains. The stronger of the two interactions (oval in Figure 4.2) is centered on a P4PE, which supports two additional C−H···N3 interactions (2.684 and 2.719 Å) per molecule thus making 4 C−H···N, 2 *ef*, and 1 *off* concerted interactions

about the inversion center at 1,0,1. The second highly concerted region (circle in

Figure 4.2) has a P8PE (Dance & Scudder, 1998) interaction about the inversion

center at 1,0,½. Since both of these regions involve a larger number of concerted

interactions, and C−H···N interactions should be stronger than *ef* interactions, the

resulting one dimensional chain should be stronger than the 6PE chains found in the

isothiocyanato and chloro complexes.
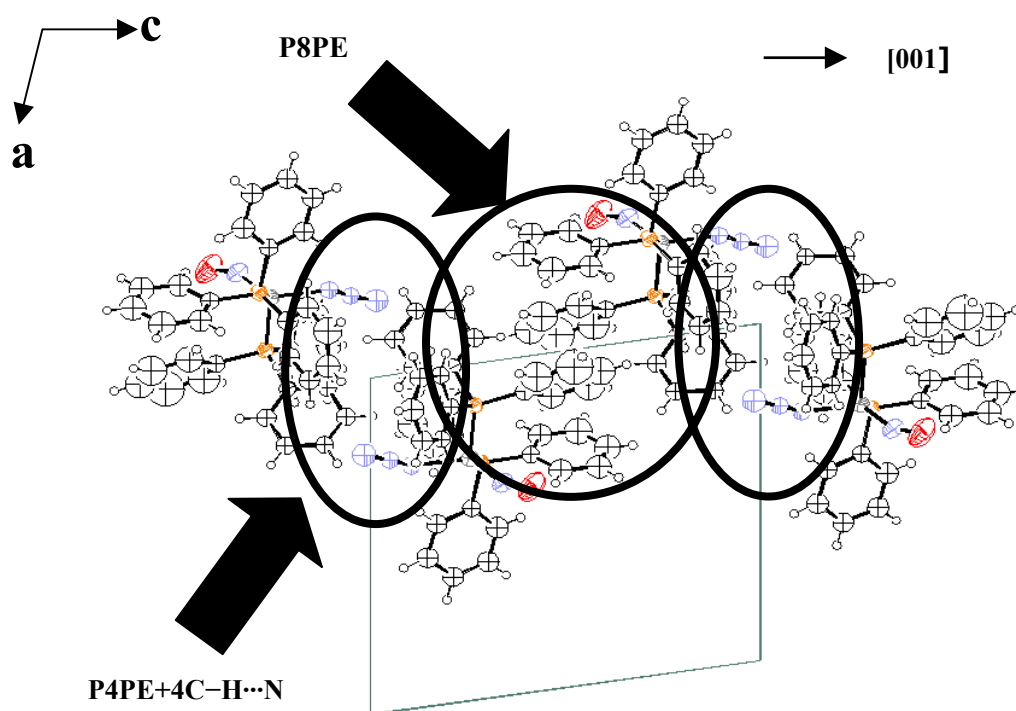
Figure 4.2. One dimensional chains of alternating P8PE and P4PE+4C−H···N. Drawn
along [001], projected on the *ac* plane.

Of course the noncovalent interactions do not occur in isolation, the actual

packing is the result of the combination of all the favorable interactions in the lattice

and the reason the 6PE do not occur in this crystal structure is a combination of the intra- and inter-molecular interactions described. The P8PE/P4PE+4C−H⋯N inter-molecular chains necessarily include the stabilizing intramolecular motifs noted by Kiatpichitpong as well.

Parallel chains are linked together in the [100] direction by the third strongest interaction to form two dimensional layers as shown by the ovals in Figure 4.3. This interaction is centered on another P4PE, with one 2.987 Å C−H⋯O interaction per molecule (2 C−H⋯O, 2 *ef*, and 1 *off*) about the inversion centers at ½,0,½.

Figure 4.4 shows an end view (projected down [001]) of the layers as shown in Figure 4.3. The one dimensional translation related chains of Figure 4.2 are highlighted with boxes, and the P4PE+2C−H⋯O chain connections with ovals.

One additional 2_1 screw axis related chain column (as in Figure 4.2) is added in Figure 4.5 to show the trigonal (hexagonal) arrangement of the columns. The boxes and solid ovals indicate the the same interactions to form layers discussed above. The dashed line ovals indicate the remaining interaction areas. There are numerous interchain interactions in these two areas, which when considered to be concerted as a group is probably as strong as the P4PE+2C−H⋯O interaction.
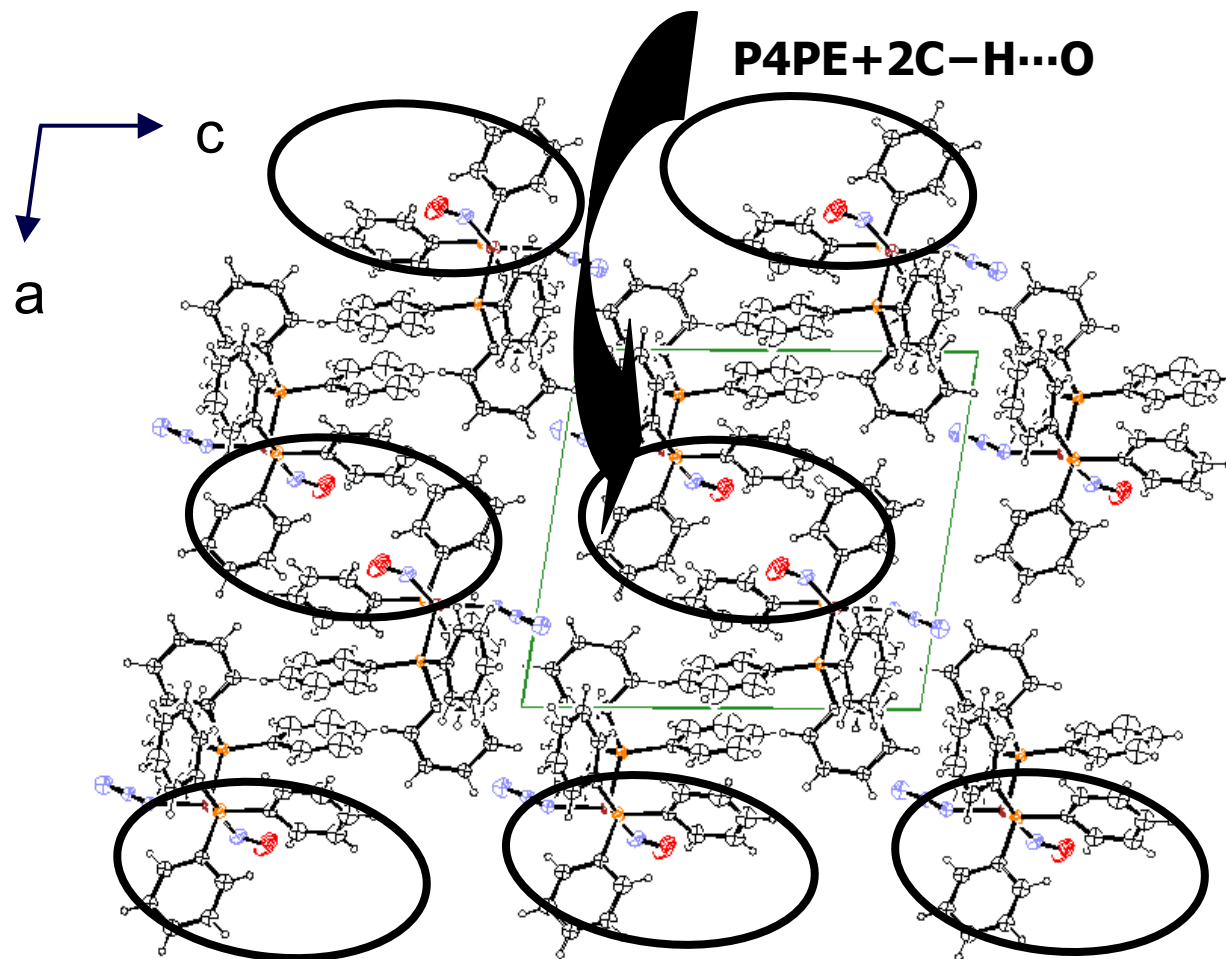
Figure 4.3. Two dimensional layers of parallel chains linked by P4PE+2C−H⋯O interactions. Oriented as illustrated in Figure 4.3.
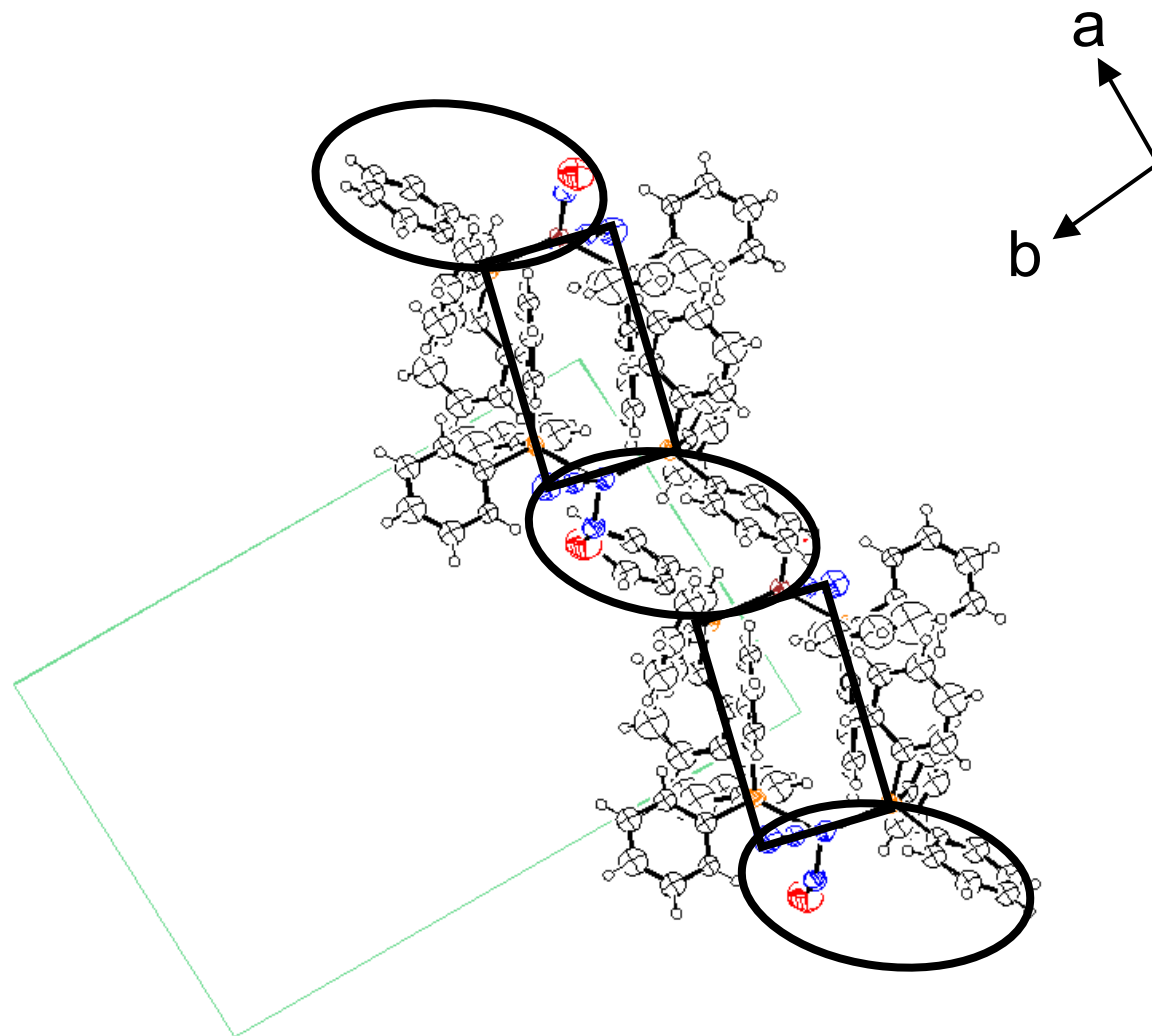
Figure 4.4. End view of the two dimensional interconnected columns. Layers from Figure 4.3.projected down [001].
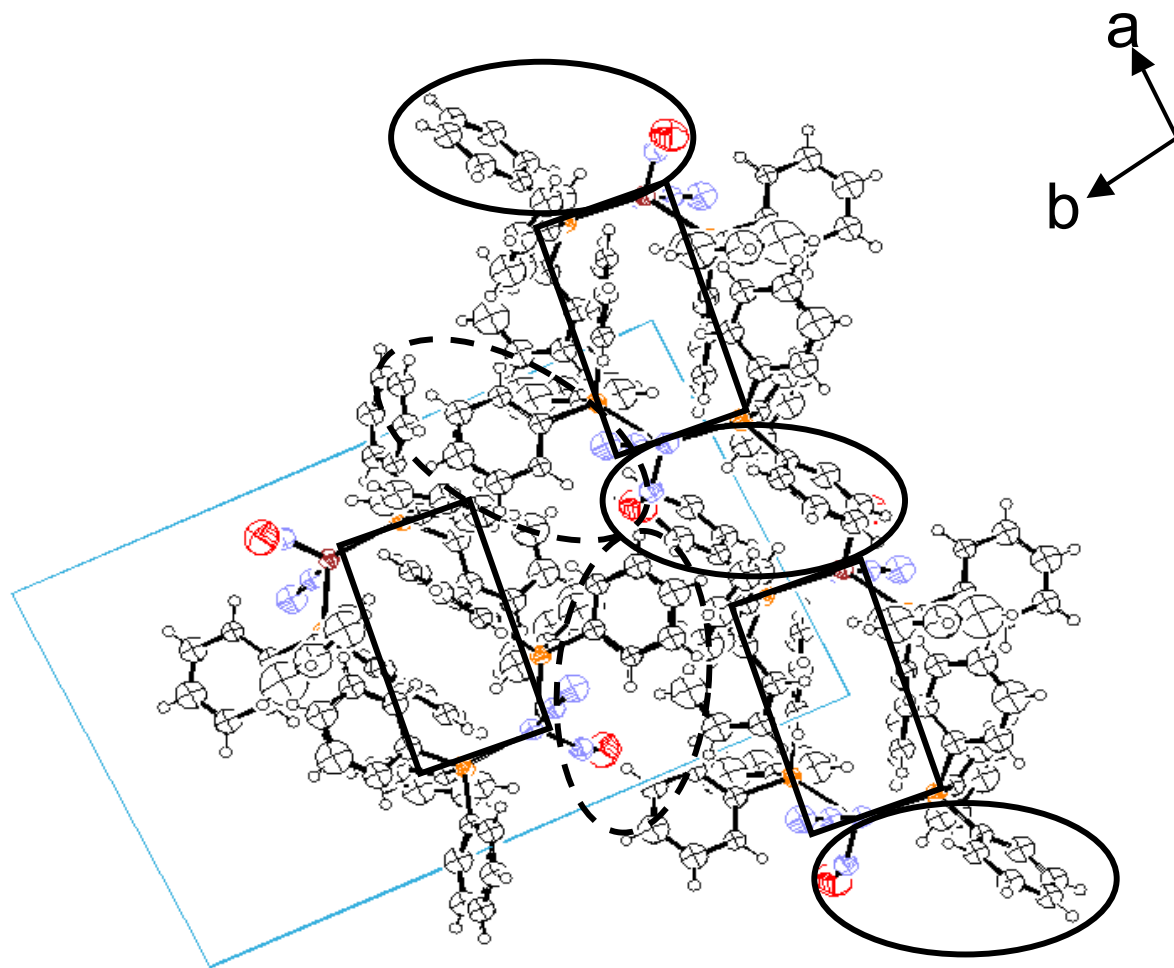
Figure 4.5. End view of the pseudo hexagonally arranged columns. Layers connections as in Figure 4.4., and interconnections indicated by dashed ovals. Columns projected down [001].

The multiple phenyl-phenyl *ef* C–H···π attractive interactions of the concerted 6PE give a sum of interaction energy sufficient to make it a dominant supramolecular motif for triphenylphosphine (TPP) complexes (Dance & Scudder, 1995). The NiX(NO)(PPh₃)₂ complexes with the fourth ligand, X = isothiocyanato, azido, or chloro, while closely related have quite different supramolecular structures.

First, the extended interactions in the isothiocycanato complex are the expected 6PE between adjacent (triphenylphosphine) TPP ligands. These interactions occur in parallel chains made up of alternating 6PE illustrated in Figure 4.6. Layers are joined together by nitrosyl-phenyl and phenyl-phenyl interactions. Thus, the three dimensional supramolecular structures is determined by a balance of concerted weak intermolecular interactions (presumably) dominated by the 6PE.

Second, the chloro complex contains distorted 6PE chains, but also a benzene solvate. The benzene molecule, able to form considerably more C−H···π interactions, becomes the major link between surrounding molecules as illustrated in Figure 4.7. Additional phenyl-phenyl interactions can be identified forming a complete three dimensional network for this complex as well.

Third, the azido complex does not form 6PE. The strongest individual nonbonded interactions are *intra*molecular C−H···N interactions to the lone pair on the N bonded to Ni. These intramolecular interactions would destroy the pseudo three-fold symmetry of the TPP ligands, thereby disrupting the possibility to form 6PE. However, a stronger set of intermolecular interactions than the SPE found in the isothiocyanato and chloro complexes has been identified. These highly concerted interactions, supplemented by the intramolecular interactions pereviously noted, most
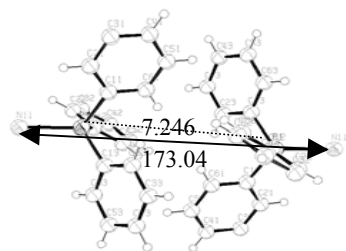
P1···P1 6PE Interaction
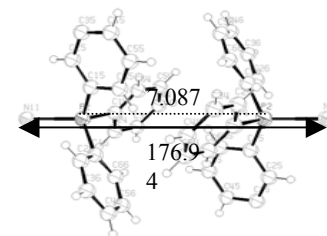
P2···P2 6PE Interaction

[-1 1 0]
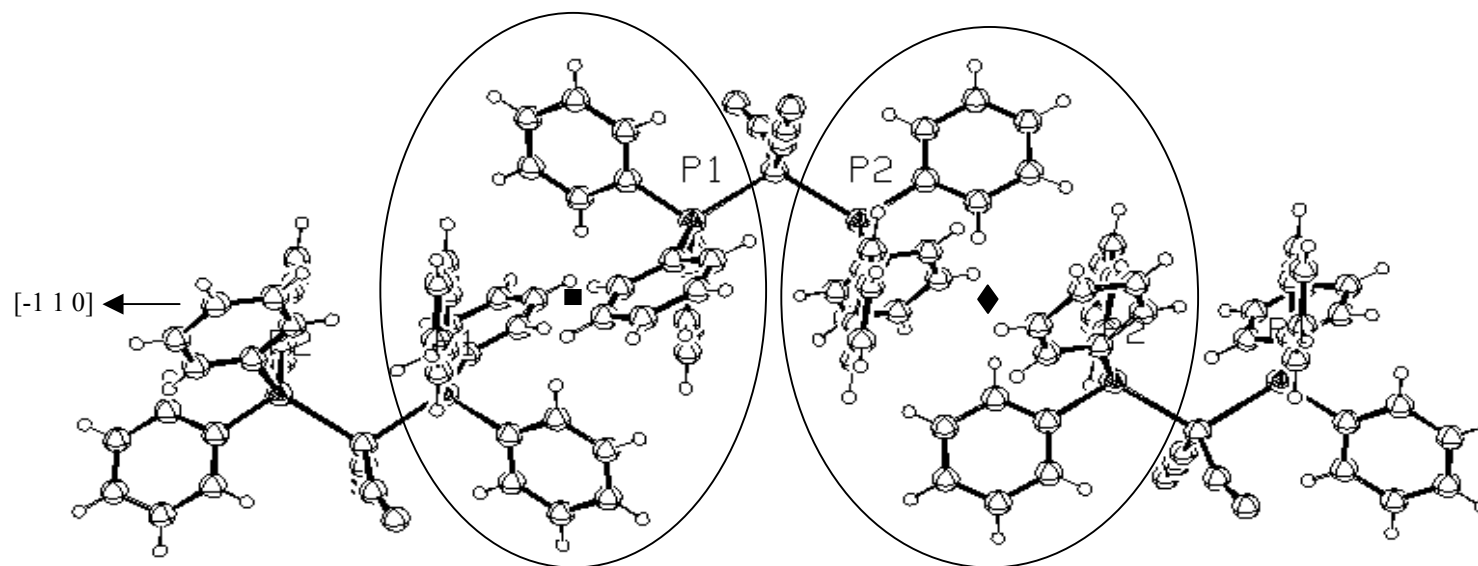
Figure 4.6. 6PE Linking Ni(NCS)(NO)(PPh$_3$)$_2$ molecules into chains (Kiatpichitpong, 2002).

■ is the inversion center at 1/2 1 1/2   ◆ is the inversion center at 1 1/2 1/2

At the height of benzene

Below the benzene
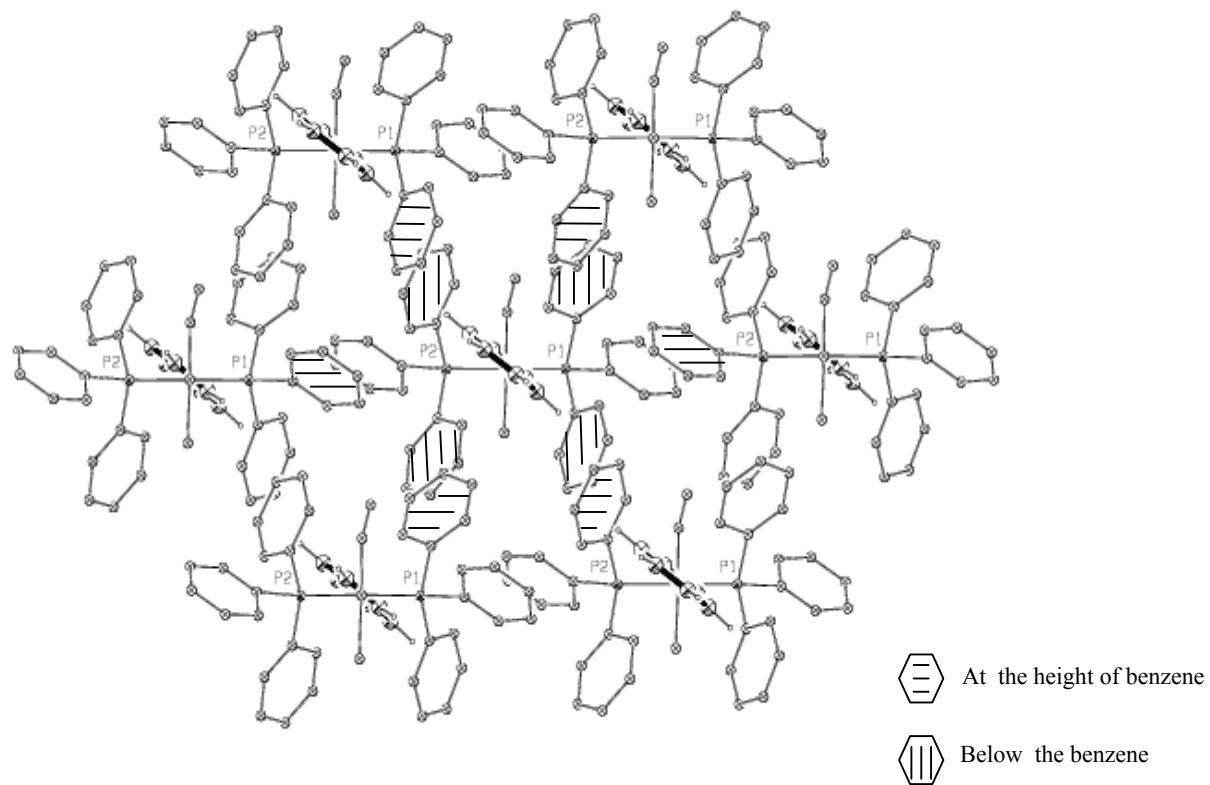
Figure 4.7. Benzene solvate in the bowl shaped cavity of NiCl(NO)(PPh$_3$)$_2$ (Kiatpichitpong, 2002).

likely dominate the supramolecular structure, and explain the absence of 6PE in the azido complex. The concerted weak noncovalent interactions can be used to explain the extended into a three-dimensional network.

4.5 Conclusions

The weak C−H⋯π and C−H⋯X interactions, especially when highly concerted can be used to explain the extended three dimensional interaction (the supramolecular structure) of the existing $Ni(X)(NO)(PPh_3)_2$ complexes. While they are closely related chemically, they have quite different forms of their supramolecular structures due to the delicate balance of the weak C−H⋯π interactions.

CHAPTER V

CONCLUSIONS AND SUGGESTIONS
FOR FUTURE WORK

5.1 Conclusions

The azido ligand geometry in the previously reported $Ni(N_3)(NO)(PPh_3)_2$ complex (Enemark, 1971) was marred by an untreated disorder problem resulting from an undetermined amount of the chloro starting material cocrystallized with the azido complex and overlapping the electron density of two of the azido nitrogen atoms.

Although the attempt to obtain a pure crystal of $Ni(N_3)(NO)(PPh_3)_2$ by synthesis from a bromo precursor was unsuccessful, an improved X-ray structure determination of the complex was still possible. The deep blue-black compound, as in the previous study, crystallizes in the monoclinic space group, $P2_1/c$, with unit cell parameters: 298 K, $a = 13.597(5)$ Å, $b = 19.098(8)$ Å, $c = 12.562(4)$ Å, $\beta = 98.59(5)°$, $V = 3221.89$ Å^3, and Z = 4. The complex cocrystallizes with 16% bromo impurity. The bromo position and occupancy, and the occupancy of the azido ligand were modeled and refined giving a chemically meaningful coordinated azido ligand model. The discrete $Ni(N_3)(NO)(PPh_3)_2$ molecules exhibit pseudo tetrahedral coordination geometry about the Ni atom with a P−Ni−P angle of 120.90(3)°, a N−Ni−N angle of 129.1(2)°, and the dihedral angle between the P−Ni−P and N−Ni−N planes of 84.7(1)°. The nitrosyl ligand parameters are normal at d[Ni−N(O)] = 1.693(3) Å,

d[N−O] = 1.129(4) Å, and d[Ni−N−O] = 152.7(3)°. All of these parameters are essentially identical to those of the previous determination.

The only significant differences in the current structure occur in the azido ligand. While the nickel-ligand distances in the previous structure were within normal ranges, the distances within the azido ligand were highly questionable. The azido ligand is nonlinearly coordinated to the Ni atom, d[Ni−N(N$_3$)] = 2.008(5) Å, and ∠[Ni−N−N] = 126.6(3)°. Including the partial bromo position in the current structure gave more reasonable structure parameters, notably d[Ni-Br] = 2.408(3) Å, d[N1−N2] = 1.150(7) Å and d[N2−N3] = 1.158(5) Å

The supramolecular structures of bis(triphenylphosphine) compounds are usually dominated by 6PE. Such 6PE were easily found for both other known compounds in this series (Kiatpichitpong, 2002). The distance/colinearity parameters for the 6PE in the isothiocyanato complex are 7.087 Å/176.9° and 7.246 Å/173.0°, while those for the chloro complex are 7.163 Å/174.2°. Although the current structure has d[P···P] of 7.350 and 7.783 Å, the colinearities are 86.98 and 117.80°, respectively and there are no 6PE in this structure.

The strongest nonbonded interaction is the 2.493 Å *intra*molecular C−H···N interaction to the lone pair on the nitrogen atom bonded to the nickel atom. The explanation for the lack of 6PE is found in a combination of intramolecular noncovalent bonding and concerted intermolecular noncovalent bonding interactions. The strongest noncovalent interaction in the structure is the 2.493 Å intramolecular C−H···N interaction mentioned above, which induces the phenyl ring involved in the interaction to be rotated to lie approximately parallel to the Ni−P vector, thereby

destroying the ideal geometry required to form a 6PE. Another strong *intra*molecular C−H⋯N interaction to the azido ligand π cloud involves the other triphenylphosphine ligand and disrupts the second possibility to form a 6PE.

At the same time, highly concerted weak C-H⋯π and C-H⋯N interactions were found in two regions, which connect the molecules together into one dimensional chains propagating in the [001] direction. The stronger of the two interactions is centered on a P4PE supported by two additional C−H⋯N_3 interactions (2.684 and 2.719 Å) per molecule thus making 4 C−H⋯N, 2 *ef*, and 1 *off* concerted interactions about the inversion center at 1,0,1. The second highly concerted region (P8PE, Dance & Scudder, 1998) has an interaction about the inversion center at 1,0,½. Since both of these regions involve a larger number of concerted interactions, and C−H⋯N interactions should be stronger than *ef* interactions, the resulting one dimensional chain should be stronger than the 6PE chains found in the isothiocyanato and chloro complexes.

The noncovalent interactions do not occur in isolation, the actual packing is the result of the combination of all the favorable interactions in the lattice and the reason the 6PE do not occur in this crystal structure is a combination of the intra- and intermolecular interactions described. The P8PE/P4PE+4C−H⋯N intermolecular chains necessarily include the stabilizing *intra*molecular motifs as well. There are numerous interactions in these two areas, which when considered to be concerted as a group is probably as strong as the P4PE+2C−H⋯O interaction. Which parallel chains are linked together in the [100] direction by the third strongest interaction to form two dimensional layers. This interaction is centered on another P4PE, with one 2.987 Å

C−H⋯O interaction per molecule (2 C−H⋯O, 2 *ef,* and 1 *off*) about the inversion centers at ½,0,½. Additional concerted interactions connect the chains into planes, and the planes into a three-dimensional network.

Thus, it is found that the weak noncovalent interactions (C−H⋯π, C−H⋯N, and C−H⋯O), especially when highly concerted, can be used to explain the extended three dimensional supramolecular structures of all three low symmetry NiX(NO)(PPh$_3$)$_2$.

5.2 Suggestions for Future Work

The synthesis of Ni(N$_3$)(NO)(PPh$_3$)$_2$ by another alternative route, perhaps from a multiatom nonhalide precursor, could lead to a pure crystal, and thus to a further improved X-ray structure determination of the complex. Some alternative conditions to try might include the following>

  (i) Increasing the reaction time;

 (ii) Changing solvent for the recrystallization;

(iii) Changing alternative route for synthesis (*e.g.* synthesis of the diazido complex for starting material or use nickel(II) nitrate hexahydrate (Ni(NO$_3$)$_2$·6H$_2$O) as starting material).

As noted in the introduction, all the metal–ligand coordination in this complex is flexible. All four ligands have varying degrees of capability to accept π back bond electron density from the metal *d* orbitals. If pure sample crystals can be produced, an electron density study would be quite interesting to examine the final valence electron density in the complex.

Metal complexation and supramolecular recognition of the polyfunctional azide anion is extremely important in biochemistry. Accessibility of series of $M(N_3)L_n$ complexes with a variety of metals like Cu, Mo, Mn, and Fe makes them amenable to systematic structural investigation to better characterize the mode of azide binding associated with the characteristic values of $d[M-N]$, $d[N-N]$, and $\angle[MNN]$, which the covalent binding significantly influences the geometry and electronic structure (Allen & Garner, 1994; Schleyer & Kos, 1983).

In finally, understanding of crystal packing into supramolecular interactions that determine the manner in which the contents of unit cells interact with the contents of other unit cells is also in progress. This research improved the structure of $Ni(N_3)(NO)(PPh_3)_2$ with single X-ray crystallographic analysis. Thus, there is evidence that a distance of interactions achieved by crystallographic method but the energy of interactions is not presented. Density functional theory (DFT) is a powerful method in electronic structure theory. In DFT, the energy of a molecule depends on the electron density. Thus, it will be use in the future to study nature the interactions within complex molecular assembly.

REFERENCES

REFERENCES

Allen, F. H., Baalham, C. A., Lommerse, P. M. J. and Raithby, P. R. (1998). Carbonyl-Carbonyl Interactions can be Competitive with Hydrogen Bonds. **Acta Crystallographica.** B54: 320-329.

Altomare, A.; Burla, M. C.; Camalli, M.; Cascarano, G. L.; Giacovazzo, C.; Guagliardi, A.; Moliterni, A. G. G.; Polidori, G.; Spagna, R. (1999). **SIR97:** A New Tool for Crystal Structure Determination and Refinement. **Journal of Applied Crystallography.** 32: 115-119.

Andres, P. R.; Schubert, U.S. (2003). Self-Assembly of Non-Helical Metallo-Supramolecular Polymers. **Polymer Preparation.** 44: 703-704.

Ayers, A. E.; Marynick, D. S.; Dias, H. V. R. (2000). Azido Derivatives of Low-Valent Group 14 Elements: Synthesis, Characterization, and Electronic Structure of [(n-Pr)$_2$ATI]GeN$_3$ Featuring Heterobicyclic 10-π-Electron Ring Systems. **Inorganic Chemistry.** 39: 4147-4151.

Bianchi, A.; Bowman-James; Garcia-Espana, E. (1997). **Supramolecular Chemistry of Anions.** Wiley-VCH, New York.

Beer, P. D.; Gale, P. A.; Smith, D. K. (1999). **Supramolecular Chemistry.** Oxford Chemistry Primers, 74. Oxford University Press.

Bein, T. (1992). **Supramolecular Architecture. Tailoring Structure and Function of Extended Assemblies.** ACS Symposium Series, Volume 499, 1-7.

Bernstein, J.; Etter, M. C. and Leiserowitz, L. (1994). **The Role of Hydrogen Bonding in Molecular Assemblies: Structure Correlation.** Volume 2, Bürgi, H.-B., Dunitz, J. D., Eds., Weinheim, New York, pages 842 & 846.

Blessing, R. H. (1995). An Empirical Correction for Absorption Anisotropy. **Acta Crystallographica.** A51: 33-38.

Bondi, A. (1964). **van der Waals Volumes and Radii**. **Journal of Physical Chemistry.** 68:3 441-451.

Brammer, L.; Stevens, E. D. (1989). Structure of Dichlorobis(triphenylphosphine) nickel(II). **Acta Crystallographica.** C45: 400-403.

Burnett, M. N.; Johnson C. K. (1996). **ORTEP-III:** Oak Ridge Thermal Ellipsoid Plot Program for Crystal Structure Illustrations, Report ORNL-6895, Oak Ridge National Laboratory, Tennessee, USA.

Cambridge Structural Database. (2001). Version 5.21, **Cambridge Crystallographic Data Centre**, 12 Union Road, Cambridge, England.

Carmalt, C. J.; Cowley, A. H.; Culp, R. D.; Jones, R. A.; Sun, Y.; Fitts, B.; Whaley, S.; Roesky, H. W. (1997). Monomeric Titanium(IV) Azides as a New Route to Titanium Nitride. **Inorganic Chemistry.** 36: 3108-3112.

Cotton, F. A.; Wilkinson, G.; Murillo C. A.; Bochmann, M. (1999). **Advanced Inorganic Chemistry**. 6th edition, Wiley Interscience, New York.

Constable, E. C. (1991). Helices, Supramolecular Chemistry and Metal-Directed Self Assembly.**Angewandte Chemie International Edition in English.** 30:111450-1451.

Cram, D. J.; Cram, J. M. (1974). Complexes Between Organic Compounds Simulate the Substrate Selectivity of Enzymes. **Science.** 183: 803-809.

Dance, I.; Scudder, M. (1995). The Sextuple Phenyl Embrace, a Ubiquitous Concerted Supramolecular Motif. **Journal of the Chemical Society, Chemical Communication.** 1039-1040.

Dance, I.; Scudder, M. (1996a). Concerted Supramolecular Motifs: Linear Columns and Zigzag Chains of Multiple Phenyl Embraces Involving Ph_4P^+ Cations in Crystals. **Journal of the Chemical Society, Dalton Transactions.** 19: 3755-3769.

Dance, I.; Scudder, M. (1996b). Supramolecular Motifs: Concerted Multiple Phenyl Embraces between Ph_4P^+ Cations are Attractive and Ubiquitous. **Chemistry: A European Journal.** 2: 481-486.

Dance, I.; Scudder, M. (1997). Dominant Cation-Cation Supramolecular Motifs in Crystals. Hexagonal Arrays of Sextuple Phenyl Embraces in Halometalate Salts of $MePh_3P^+$. **Journal of the Chemical Society, Dalton Transactions.** 2019-2027.

Dance, I.; Scudder, M. (1998). Crystal Supramolecularity: Elaborate Six-, Eight- and Twelve-Fold Concerted Phenyl Embraces in Compounds $[M(PPh_3)_3]^z$ and $[M(PPh_3)_4]^z$. **New Journal of Chemistry.** 481-492.

Dance, I.; Scudder, M. (2000). Crystal Supramolecularity: Sixfold Phenyl Embraces between PPh_3 Ligands, Forming Extended Nets in One-, Two-, and Three Dimensions**. Journal of the Chemical Society, Dalton Transactions.** 1587-1594.

Drago, R. S. (1992). **Physical Methods for Chemists.** 2nd Edition. Saunders College Publishing, pages 689-691.

Duisenberg, A. J. M.; Kroon-Batenburg, L. M. J.; Schreurs, A. M. M. (2003). An intensity evaluation method: EVAL−14. **Journal of Applied Crystallography.** 36: 220-229.

Enemark, J. H. (1971). Four-Coordinate Metal Nitrosyls. 1. The Structure of Azidonitrosylbis(triphenylphosphine)nickel $Ni(N_3)(NO)(PPh_3)_2$. **Inorganic Chemistry.** 10:9. 1952-1957.

Enemark, J. H.; Feltham, R. D. (1974). Principles of Structure, Bonding, and Reactivity for Metal Nitrosyl Complexes. **Coordination Chemical Reviews.** 13: 339-406.

Enemark, J. H., Feltham, R. D., Riker-Nappier, J. & Bizot, K. F. (1975). Stereo-chemical Control of Valence IV. Comparison of the Structures and Chemical Reactivities of Five and Six-Coordinate Complexes of the $\{CoNO\}^8$ Group. **Inorganic Chemistry.** 14: 624-632.

Epstein, M. A. F. (1982). **Nucleation, Growth and Impurity Effects in Crystallization Process Engineering.** American Institute of Chemical Engineers, New York.

Farrugia, L. J. (1997). ORTEP-3 for Windows - a version of ORTEP-III with a Graphical User Interface (GUI). **Journal of Applied Crystallography.** 30: 565.

Ferraro, J.; Krishhmann, K. (1990). **Practical Fourier Transform Infrared Spectroscopy.** 1st edition, Academic Press, New York.

Feltham, R. D. (1964). Metal Nitrosyls. I. Triphenylphosphine Nitrosyl Nickel Complexes. **Inorganic Chemistry.** 3: 116-122.

Goher, M. A. S.; Mautner, F. A.; Abu-Youssef, M. A. M.; Hafez, A. K.; Badr, A. M.-A. (2002). Synthesis and Crystal Structure of Three New 2D Polymeric Cadmium(II) Complexes of Some Pyridine Derivatives with Different Cadmium(II) Azide Topologies. **Journal of the Chemical Society, Dalton Transactions.** 3309-3312.

Gohy, J. F. M. W.; Lohmeijer, B. G. G.; Schubert, U. S. (2003). From Supra-molecular Block Copolymers to Advanced Nano-objects, **Chemistry: A European Journal.** 9: 3472-3479.

Griffiths, P. R.; de Haseth, J. A. (1986). **Fourier Transform Infrared Spectroscopy.** Wiley, New York.

Gunzler, H.; Gremlich, H.-U. (2002). **IR Spectroscopy: An Introduction.** Wiley-VCH, Cambridge.

Haller, K. J. (1978). Structural Studies of the Binding of Small Molecules to Transition Metals. **Ph. D. Dissertation**, The University of Arizona, Tucson AZ, USA.

Haller, K. J.; Enemark, J. H. (1978). Four-Coordinate Metal Nitrosyls. 2. Structures of $NiX(NO)(PPh_3)_2$ Complexes. **Inorganic Chemistry.** 17:12. 3552-3558.

Hammond, C. (1997). **The Basics of Crystallography and Diffraction.** International Union of Crystallography, Oxford University Press, New York.

Hossain, M. A.; Schneider, H.-J. (1999). Supramolecular Chemistry Part 85. **Chemistry: A European Journal.** 5: 1284-1290.

Huheey, J. E.; Keiter, E. A.; Keiter, R. L. (1993). **Inorganic Chemistry: Principles of Structure and Reactivity.** 6th edition, Harper Collins College, New York, pages 585, 634.

Hunter, C. A.; Sanders, J. K. M. (1990). The Nature of π-π Interaction. **Journal of the American Chemical Society.** 112: 5525-5534.

IUCr (2003). *cif* **Core Dictionary**, version 2.3, International Union of Crystallography, Chester, England.

Jones, W.; Rao, C. N. R. (2002). **Supramolecular Organization and Materials Design.** Cambridge University Press.

Kashchiev, D. (2000). **Nucleation.** Butterworth-Heinemann, Boston.

Khosavithitkul, N; Haller, K. J. (2003). **Supramolecular Interactions in Four-Coordinate Azidonitrosylbis(triphenylphosphine)nickel.** Proceedings, Tenth Tri-University Conference, Chiang Mai, 212-215.

Kiatpichitpong, A. (2002). Supramolecular Structures of Four-Coordinate Nickel Nitrosyl bis(Triphenylphosphine) Complexes. **M. Sc. Thesis**, Suranaree University of Technology, Nakhon Ratchasima, Thailand.

Kilbourn, B. T.; Powell, H. M. (1970). Allogons: Isomerism in The Crystal and Molecular Structure of the Green Form of Dibromobis(benzyldiphenyl phosphine)nickel(II) Ni[P(CH$_2$Ph)Ph$_2$]$_2$Br$_2$[square], 2Ni[P(CH$_2$Ph)Ph$_2$]$_2$Br$_2$[tetra hedral]. **Journal of the Chemical Society Section A.** 1688-1693.

Klug, A. (1983). From Macromolecule to Biological Molecular Assembly. **Angewandte Chemie International Edition in English.** 22: 565-582.

Kriege-Simondsen, J.; Elbaze, G.; Dartiguenave, M.; Feltham, R. D.; Dartiguenave, Y. (1982). Oxygen Atom Transfer Reactions. 2. Reaction of Carbonmonoxide withNi(NO$_2$)$_2$(PMe$_3$)$_2$ Structure of Nitrosylbis(trimethylphosphine)nickel, Ni(NO$_2$)(NO)(PMe$_3$)$_2$. **Inorganic Chemistry.** 21: 230-236.

Lehn, J.-M. (1973). Design of Organic Complexing Agents: Strategies Towards Properties. **Structural Bonding.** 16: 1-69.

Lehn, J.-M. (1995). **Supramolecular Chemistry: Concepts and Perspectives**. VCH.

Ma, J. C.; Dougherty, D. A. (1997). The Cation−π Interaction. **Chemical Reviews.** 97: 303-1324.

Manikandan, P.; Muthukumaran, R.; Thomas, K. R. J.; Varghese, B.; Chandramouli, G. V. R.; Manoharan, P. T. (2001). Copper(II) Azide Complexes of Aliphatic

and Aromatic Amine Based Tridentate Ligands: Novel Structure, Spectroscopy, and Magnetic Properties. **Inorganic Chemistry.** 40: 2378-2389.

Markov, I. V. (2003). **Crystal Growth for Beginners: Fundamentals of Nucleation, Crystal Growth and Epitaxy.** 2nd edition, World Scientific.

Massoud, S. S.; Mautner, F. A.; Abu-Youssef, M. A. M.; Shuaib, N. M. (1999). Synthesis and Characterization of Binuclear and Polymeric Five-Coordinate Copper(II) Complexes Derived from 3,3′,3″-triaminotripropylamine (trpn) Crystal Structure of $[Cu(trpn)(N_3)]ClO_4$ and $Cu_2(trpn)(tren)(NO_2)(H_2O)]$ $(ClO_4)_3$. **Polyhedron.** 18: 2061-2067.

Mullin, J. W. (2001). **Crystallization.** 4th edition, Oxford.

Müller-Dethlefs, K.; Hobza, P. (2000). Noncovalent Interactions: A Challenge for Experiment and Theory. **Chemical Reviews.** 100:1. 143-167.

Nakamoto, K. (1997). **Infrared and Raman Spectra of Inorganic and Coordination Compounds.** 5th edition, Wiley.

Nishio, M.; Hirota, M. (1989). CH/π Interaction: Implications in Organic Chemistry. **Tetrahedron.** 45:23. 7201-7245.

Nonius BV. (1998). **COLLECT: KappaCCD software**, Nonius BV, Delft, The Netherlands.

Ohtaki, H. (1998). **Crystallization Process.** Wiley, New York.

Orpen, G. A.; Connelly, N. G. (1985). Structure Evidence for the Participation of P−X σ^* Orbitals in Metal-PX$_3$ Bonding. **Journal of the Chemical Society, Chemical Communications.** 1310-1311.

Pauling, L. (1948). **The Nature of the Chemical Bond** 2nd edition, Cornell University Press, New York.

Palo, D. R.; Erkey, C. (1998). Solubility of Dichlorobis(triphenylphosphine)nickel(II) in Supercritical Carbon Dioxide. **Journal of Chemical and Engineering Data.** 43: 47-48.

Pedersen, C. J. (1967). Cyclic Polyethers and Their Complexes with Metal Salts**. Journal of the American Chemical Society.** 89: 7017-7036.

Rowland, R. S.; Taylor, R. (1996). Intermolecular Nonbonded Contact Distances in Organic Crystal Structures: Comparison with Distances Expected from van der Waals Radii. **Journal of Physical Chemistry.** 100: 7384-7391.

Schleyer, P. R.; Kos, A. J. (1983). The Importance of Negative (Anionic) Hyperconjugation. **Tetrahedron.** 39:7 1141-1150.

Schneider, H.-J.; Yatsimirsky, A. (2000). **Principles and Methods in Supramolecular Chemistry.** Wiley, England.

Scudder, M.; Dance, I. (1998). Crystal Supramolecular Motifs. Ladders, Layers and Labyrinths of Ph_4P^+ Cations Engaged in Fourfold Phenyl Embraces. **Journal of the Chemical Society, Dalton Transactions.** 3155-3165.

Sheldrick, G. M. (1997). **SHELXL97. Program for the Refinement of Crystal Structures.** University of Göttingen, Germany.

Shriver, D. F.; Drezdzon, M. A. (1986). **The Manipulation of Air-Sensitive Compounds.** 2nd edition, Wiley.

Skoog, D. A.; Leary, J. J. (1992). **Principles of Instrumental Analysis.** 4th edition, Saunders College Publishing, Philadelphia. 113-120, and 266-270.

Stamler, J. S.; Feelisch, M. (1996). Biochemistry of Nitric Oxide and Redox Related Species, in **Methods in Nitric Oxide Reseach.** Feelisch & Stamler, Eds, Wiley, 19-28.

Steed, J. W.; Atwood, J. L. (2000). **Supramolecular Chemistry.** Wiley, England.

Steiner, T. (1997). Unrolling the Hydrogen Bond Properties of C−H···O Interactions. **Journal of the Chemical Society, Chemical Communications.** 727-734.

Steiner, T. (1998). Donor and Acceptor Strengths in C−H···O Hydrogen Bonds Quantified from Crystallographic Data of Small Solvent Molecules. **New Journal of Chemistry.** 1099-1103.

Steiner, T.; Desiraju, G. R. (1998). Distinction between the Weak Hydrogen Bond and the van der Waals Interaction. **Journal of the Chemical Society, Chemical Communications.** 891-892.

Taylor, R.; Kennard, O. (1982). Crystallographic Evidence for the Existence of C−H···O, C−H···N, and C−H···Cl Hydrogen Bonds. **Journal of the American Chemical Society.** 104: 5063-5070.

Tchertanov, L. (2000). Understanding the Peculiarities of Azide and Thiocyanate Binding in Proteins. Use of the Small Molecule Structural Data. **Supramolecular Chemistry.** 12: 67-91.

Venanzi, M. L. (1958). Tetrahedral Nickel(II) Complexes and the Factors Determining Their Formation: Part I. Bistriphenylphosphine Nickel(II) Compounds. **Journal of the Chemical Society.** 719-724.

Xiao, S-X.; Trogler, W. C.; Ellis, D. E.; Berkovich-Yellin, Z. (1983). Theoretical Study of the Frontier Orbitals of Metal-Phosphine Complexes. **Journal of the American Chemical Society.** 105: 7033-7040.

Zigler, S. S.; Haller, K. J.; West, R.; Gordon, M. S. (1989). Structures of Two Organosilyl Azides. **Organometallics.** 8: 1656-1660.

APPENDICES

APPENDIX A

ORTEP INSTRUCTION FORMAT

The crystal structure illustrations were drawn using the Oak Ridge Thermal Ellipsoid Plot program ORTEP-III (Burnett & Johnson, 1996). The ORTEP-III program presents illustrations in which each atom can be represented as a sphere with arbitrary radius, or as a (user specified probability) surface determined by the atomic displacement parameters from the least squares refinement. Bond radii are also specified by the user, and the program has the capability to deal with the hidden line problem for all atoms, bonds, or other features included in the drawing. Another useful feature of the program is the interatomic length and angle calculation feature. These instructions (see below) do an extensive calculation of all distances from an origin atom to all specified atoms in all possible symmetry positions in a ± two unit cell volume from the origin atom. This brute force calculation is a very effective method when looking for weak interactions.

The full functionality of the program can be realized by running it from prepared instruction files as described in Burnett and Johnson (1996). The original program has been adapted to an interactive environment by adding a graphic user interface. This seemingly more convenient, but somewhat restricted version (*e.g.* allowed rotations cannot be fractions of degrees, and the default projections for packing diagrams are perpendicular to real cell directions) of the program is also available (Farrugia, 1997).

The crystal and coordinate data used for all ORTEP calculations was taken from the least squares refinement reported in Chapter IV. The hydrogen atom positions were idealized with d[C−H] = 0.95 Å.

A sample input instruction file for the ORTEP-III program, with the traditional formatting, is given in Table A.1. The data input consists of five types of information as follows:

1. Title. The first line of input is a job title.

2. Cell parameters are provided on the second line.

3. The symmetry operators of the space group begin on line 3 of the input and continue as needed. The final symmetry operator instruction must have a digit 1 in the first column of the line as a flag to the program that all the symmetry operators have been given..

4. Atomic parameters for each atom, provided as two lines per atom: the first line gives the name and the positional parameters of the atom, and the second line gives its isotropic or anisotropic atomic displacement parameters.

5. Command instructions used to add or subtract atom positions for plotting, to select plot origin and to rotate, position, and scale the subject for projection onto the drawing surface, to add lines to represent cell edges in packing diagrams, and to represent the bonds and atoms in a variety of styles to help make clear the relationships of the various components of the illustration.

Definitions

Calculations are started from an atom or a group of atoms (molecule, sphere of enclosure, or box of enclosure). When searching for atoms within some distance of an origin atom, the origin atom is represented by an *atom designator code* (ADC),

NNTTTSS, where NN represents the serial position of a set of atom coordinates in the input list of atoms, TTT represents translations in the **a**, **b**, and **c** unit cell directions as described below, and SS represents the serial position of a symmetry operation in the input list of symmetry operators. The ADC is used to specify a particular atom in the crystal and is decoded into five components by ORTEP according to the following equation:

$$ADC = AN*10^5 + (TA + 5)*10^4 + (TB + 5)*10^3 + (TC + 5)*10^2 + SN$$

Where: AN = *atom number* $(0 \leq AN \leq NATOM \leq 500)$ - the numerical position of the atom in the input list of atoms in the asymmetric unit, which contains NATOM atoms. Atom 0 is not in the input atom list but refers to the crystal origin point (0.,0.,0.).

TA, TB, TC = *crystal lattice translation digits* – translations along cell edges **a**, **b**, and **c**, respectively. Each digit in an ADC can range from 1 to 9 with 5 representing zero translation; consequently, it is possible to move up to 4 cells in any direction from the origin cell 555. A similar definition of cell translations has been adopted by the International Union of Crystallography in their definitions of terms for the crystallographic information file, *cif* (IUCr, 2003).

SN = *symmetry operator number* $(0 \leq SN \leq NSYM \leq 96)$ – the numerical position of the symmetry operator in the input list of symmetry operators, which contains NSYM entries. Symmetry operator number 0 is not in the input list but refers to an identity operator. However, the identity operation (corresponding to position x, y, z) generally must be somewhere in the input symmetry operator list and is usually the first operator.

Example: An atom designator code of 347502 refers to atom 3 moved through symmetry operation 2, then translated −1 cell translation along **a**, +2 cell translations along **b**, and 0 cell translations along **c**.

An A*tom Designator Run (ADR)* is a straight run sequence of atoms that is defined using two atom designator codes with a "-" preceding the second of the two. The run hierarchy is: first, atom number, AN; second, symmetry operator number, SN; third, **a** translation, TA; fourth, **b** translation, TB; and last, **c** translation, TC.

Example: ADR (145502-245603) will generate the 8-atom run; 145502, 245502, 145503, 245503, 145602, 245602, 145603, 245603.

The following exceptions are allowed in origin ADRs of instructions 101, 102, 402/412, 403/413, and 404/414 only:

- The "-" may be deleted from the second ADC.

- If the second atom in the atom designator run has the same symmetry and translation components as the first atom, the second atom may be represented by its atom number component alone.

Example: ADR (345502-745502) may also be represented as(345502 745502), (345502-7), or (345502 7). ADR (355501-755501) may also be represented as (355501 755501) or (355501 7) or (3 7).

An *Atom Number Run (ANR)* is a subset of the atom designator run in which only the atom number AN changes. Normally, an ANR is entered by using only the atom number values for the first and last member of the sequence without a "-".

Example: (1 4) will designate atoms 1, 2, 3, and 4 of the input list.

A *Vector Designator Code (VDC)* defines a vector using two atom designator codes. The vector direction is from the first to the second.

Example: 253704 263704 is a vector along the positive **a** direction of the crystal lattice.

A *Vector Search Code* consists of two number runs and a distance range. It is used for finding interatomic distances that have a particular chemical significance, such as covalent and coordination bonds.

Example: Suppose that metal atoms are numbers 1 and 2 in the atom list, oxygen atoms are 6-12, and the interatomic distance range between metal atoms and oxygen atoms is 1.9 Å to 2.4 Å. The metal-to-oxygen vectors can be specified by the vector search code (1 2) (6 12) (1.9 2.4). Several variations of this basic code are used in ORTEP.

Instruction Input

1. Structure Analysis Instructions (100 Series)

The 100 series of instructions is not connected with drawing illustrations but rather with obtaining a convenient tabulation of the chemically interesting aspects of a crystal structure, including interatomic distances and angles and principal axes of thermal motion. If the ORTEP output is omitted, these instructions do nothing.

Instructions 101 and 102

These instructions find all "target" atoms within a sphere of enclosure of radius D_{max} about a particular origin atom. The instruction card has an atom designator run of one or several origin atoms and an atom number run of target atoms. The origin ADR allows calculation of several spheres successively with a printout of results after each sphere. One must be cautious, as the maximum number of results to be stored in the output list is 25. Thus, if D_{max} is made too large, only the 25 shortest distances are retained in the output list.

A 101 instruction is used to obtain a tabulation of the atoms surrounding one atom or a series of several designated atoms.

Example: If the phosphorous atoms are numbers 42 and 43 in the input list and the nickel atom is number 44 in the input list, to obtain a list of all P−P and P−Ni contacts out to a distance of 12 Å about each of the two phosphorus atoms, the following 101 instruction would be used.

$$101(102) \quad \underbrace{4255501 \quad 4355501}_{(a)} \quad \underbrace{42 \quad 44}_{(b)} \quad \underbrace{12}_{(c)}$$

where: (a) is the origin atoms 42 through 43 of symmetry operation 1,

(b) is the target atoms 42 through 44 of all symmetry operations, and translation operations ± two unit cell translations along **a**, **b**, and **c**, and

(c) D_{max}, the maximum distance to retain in the output listing of 12 Å.

A 102 instruction gives both interatomic distances and interatomic angles. The caution noted above with the 101 instruction also applies here. If there are more than 25 distances within the range, interatomic angles will only be calculated among the 25 positions listed. In this case, it may be necessary to divide the target range into two or more ranges and examine the output carefully to select the final calculation instruction to get all the required distances and angles. The 101 instruction example above is analogous to the 102 instruction to obtain a list of all P−P and P−Ni contacts, and the associated interatomic P−P−P and Ni−P−P angles for contacts less than 12 Å about each of the two phosphorus atoms.

2. Atoms Array Control Instructions (400 Series)

This series allows the user to specify which atoms are to be included in the illustration. Atoms can be added to the array, or subtracted from the array. The atom designators for the chosen atoms are stored in the ATOMS array for future use by other instructions.

Instruction 401

Group of atoms are added to the ATOMS array. The group can be denoted by atom designator codes, atom designator runs, spheres of atoms about any center point, and boxes of atoms centered on any point. Duplicate entries of the same atomic position are detected by program and only stored in the array once. Iterative sphere of enclosure adds are allowed, enabling construction of a molecule or other fragment based on chemical bonding information. The 400 series instructions are cumulative, *i.e.* any 400 series instruction will add (or subtract) atoms to (from) those already in the atoms array from previous 400 series instructions. The 400 series of instructions may contain:

(a) atom designator codes for single atoms;

(b) atom designator runs for several atoms in a run;

(c) blank fields (except between the two entries of a run);

(d) any combinations of (a), (b), and (c).

For example:

401   155501 -7455501   146501 -7446501

401   164501 -7464501 7556501 7545501

Table A.1. Crystal Data and Nonhydrogen Coordinates for NiN$_3$(NO)(PPh$_3$)$_2$.
Compound Name: Azido-nitrosyl-bis(triphenylphosphine) nickel
Empirical Formula: C36 H30 N4 Ni1 O1 P2
Unit Cell: 12.5606 19.0917 13.5874 90.0 98.574 90.0
Cell Errors: 0.0008 0.0010 0.0005 0.0 0.005 0.0
Z: 4
Space Group: P2$_1$/c
Symmetry Operators: +X,+Y,+Z; -X+1/2, +Y+1/2, -Z; -X,-Y,-Z; +X+1/2, -Y+1/2, +Z
Atom Coordinates: (Atom Name, fractional x, fractional y, fractional z)

Atom	x	y	z
C11	0.99899	0.08782	0.78835
C21	1.01307	0.07755	0.89044
C31	1.10471	0.04386	0.93735
C41	1.18003	0.01977	0.88302
C51	1.16647	0.02897	0.78269
C61	1.07586	0.06364	0.73419
C12	0.88138	0.21454	0.79387
C22	0.78864	0.24447	0.81647
C32	0.79151	0.30733	0.86680
C42	0.88782	0.34063	0.89344
C52	0.98016	0.31172	0.87124
C62	0.97811	0.24840	0.82117
C13	0.89473	0.14663	0.60470
C23	0.93401	0.20729	0.57345
C33	0.94848	0.21571	0.47609
C43	0.92465	0.16369	0.40939
C53	0.88820	0.10234	0.43877
C63	0.87102	0.09286	0.53586
C14	0.70533	-0.07242	0.58824
C24	0.75991	-0.13132	0.56443
C34	0.75542	-0.15161	0.46656
C44	0.69527	-0.11487	0.39189
C54	0.64130	-0.05633	0.41363
C64	0.64695	-0.03482	0.51126
C15	0.57116	-0.07395	0.74019
C25	0.50295	-0.11409	0.67464
C35	0.44153	-0.07825	0.85277
C45	0.37465	-0.11854	0.78728
C55	0.40458	-0.13599	0.69762
C65	0.53864	-0.05416	0.82936
C16	0.79631	-0.10239	0.78876
C26	0.76545	-0.15990	0.83886
C36	0.84375	-0.20358	0.89093
C46	0.94879	-0.19084	0.89242
C56	0.98147	-0.13309	0.84435
C66	0.90529	-0.08923	0.79352
N1	0.72153	0.06693	0.89468
N2	0.74810	0.10877	0.95000
N3	0.77322	0.14727	1.01560
N4	0.63264	0.11830	0.65928
Ni1	0.71952	0.07406	0.74386
O1	0.60964	0.14559	0.58567
P1	0.87458	0.12961	0.73180
P2	0.70231	-0.04385	0.71537

Table A.2. Calculated Hydrogen Atom Coordinates for NiN$_3$(NO)(PPh$_3$)$_2$.

H21	-0.96117	0.09320	0.92745
H31	1.11479	0.03771	1.00601
H41	1.24102	-0.00309	0.91477
H51	0.72303	0.22207	0.79759
H61	1.21797	0.01203	0.74619
H22	1.06735	0.07040	0.66568
H32	0.72837	0.32692	0.88250
H42	0.89015	0.38323	0.92689
H52	1.04539	0.33465	0.88982
H62	1.04158	0.22889	0.80610
H23	0.95139	0.24369	0.61846
H33	0.97512	0.25792	0.45580
H43	0.93347	0.17034	0.34328
H53	0.87436	0.06584	0.39334
H63	0.84365	0.05061	0.55522
H24	0.79991	-0.15743	0.61468
H34	0.79379	-0.19078	0.45121
H44	0.69116	-0.12978	0.32627
H54	0.60077	-0.03095	0.36287
H64	0.61094	0.00563	0.52560
H25	0.52317	-0.12672	0.61396
H35	0.42151	-0.06684	0.91399
H45	0.30924	-0.13401	0.80351
H55	0.35877	-0.16258	0.65212
H65	0.58184	-0.02487	0.87316
H26	0.69278	-0.16965	0.83805
H36	0.82250	-0.24211	0.92509
H46	0.99974	-0.22110	0.92604
H56	1.05440	-0.12373	0.84615
H66	0.92758	-0.04992	0.76170

APPENDIX B

SUPPLEMENTARY MATERIAL FOR NI(N₃)(NO)(PPH₃)₂

Table B.1. Fractional Monoclinic Coordinates[a] and Isotropic Atomic Displacement Parameters[b] for the Nonhydrogen Atoms in $Ni(N_3)(NO)(PPh_3)_2$ ($Å^2$).

Atom[c]	x	y	z	U_{eq}
Ni	0.71957(3)	0.074031(19)	0.74390(3)	0.03696(11)
Br	0.7248(2)	0.08718(17)	0.9214(2)	0.0488(10)
N1	0.7222(3)	0.0658(2)	0.8916(4)	0.0560(14)
N2	0.7480(2)	0.10851(19)	0.9501(2)	0.0293(6)
N3	0.7728 (4)	0.1469(2)	1.0155(3)	0.0697(12)
P1	0.87459(6)	0.12957(4)	0.73174(5)	0.03481(17)
P2	0.70224 (7)	-0.04387(4)	0.71531(6)	0.03826(18)
N4	0.6323 (2)	0.11834(15)	0.6592(2)	0.0526(7)
O4	0.6093(3)	0.14557(18)	0.5853(3)	0.1016(12)
C6	0.8814(2)	0.21455(14)	0.7936(2)	00363(6)
C8	0.9990(2)	0.08775(14)	0.7884(2)	0.0361(6)
C9	0.7967(3)	-0.10227(28)	0.7891(2)	0.0414(7)
C10	0.7049(3)	-0.07251(16)	0.5880(2)	0.0414(7)
C12	0.7886(3)	0.24452(15)	0.8164(2)	0.0413(7)
C13	0.8946(3)	0.14632(17)	0.6046(2)	0.0428(7)
C14	1.0759 (3)	0.06366(15)	0.7341(2)	0.0435(7)
C15	1.0136 (3)	0.07746(17)	0.8904(2)	0.0438(7)
C16	0.9053(3)	-0.08913(17)	0.7932(3)	0.0479(8)
C17	0.9779(3)	0.24863(18)	0.8212(3)	0.0555(9)
C18	0.5710(3)	-0.07376(16)	0.7405(2)	0.0444(7)
C19	1.1798 (3)	0.01947 (17)	0.8830(3)	0.0487 (8)
C20	1.1661 (3)	0.02900 (17)	0.7825(3)	0.0500(8)
C21	1.1045(3)	0.04379(18)	0.9376(3)	0.0495(8)
C22	0.5384(3)	-0.0546(2)	0.8292(3)	0.0581(9)
C23	0.9490(4)	-0.1904(2)	0.8925(3)	0.0657(11)
C24	0.9804(3)	0.31166(19)	0.8713(3)	0.0671(11)
C25	0.7653(3)	-0.16014(18)	0.8388(3)	0.0592(9)
C26	0.5027(3)	-0.1140(2)	0.6745(3)	0.663(11)
C27	0.7917(3)	0.30742(17)	0.8669(3)	0.0511(8)

Table B.1. (Continued).

Atom[c]	x	y	z	U_{eq}
C28	0.6416(4)	-0.0567(2)	0.4139(3)	0.0664(11)
C29	0.8429(4)	-0.20370(19)	0.8906(6)	0.0719(12)
C30	0.9335(4)	0.2074(2)	0.5730(3)	0.0748(13)
C31	0.6470(3)	-0.03490(19)	0.5112(3)	0.0560(9)
C32	0.7546(4)	-0.1520(2)	0.4664(3)	0.0781(13)
C33	0.3750(4)	-0.1185(2)	0.7880(4)	0.0759(12)
C34	0.6949(4)	-0.1153(2)	0.3922(3)	0.0733(12)
C35	0.9815(3)	-0.1331(2)	0.8443(3)	0.0584(9)
C36	0.7598(3)	-0.1313(2)	0.5646(3)	0.0628(10)
C37	0.8877(3)	0.34O44(18)	0.8939(3)	0.0585(9)
C39	0.4414(3)	-0.0780(2)	0.8526(3)	0.0714(11)
C40	0.4050(4)	-0.1361(2)	0.6985(4)	0.0855(14)
C41	0.8711(4)	0.0933(2)	0.5362(3)	0.0780(13)
C44	0.8879(5)	0,1026(3)	0.3935	0.109
C46	0.9491(5)	0.2160(3)	0.4760(4)	0.1023(19)
C47	0.9251(4)	0.1643(3)	0.4092(3)	0.0921(16)

[a] Estimated standard deviations of the least significant digits are given in parentheses.

[b] Equivalent isotropic atomic displacement parameters for the atoms refined anisotropically.

[c] The bromine position represents an impurity in the azido crystal. The refined occupancy of bromine is 0.164(3). The occupancy of the nitrogen atoms of the azido group was also refined with the constraint that the sum of the two occupancies must be equal to unity.

$U_{eq} = 1/3(U_{11}+U_{22}+U_{33})$

Table B.2. Anisotropic Atomic Displacement Parameters[a] in Ni(N$_3$)(NO)(PPh$_3$)$_2$ (Å^2).

Atom	U_{11}	U_{22}	U_{33}	U_{23}	U_{13}	U_{12}
Ni	0.0382(2)	0.03256(19)	0.0406(2)	-0.00200(16)	0.00721(16)	-0.00071(16)
N3	0.094(3)	0.060(2)	0.056(2)	-0.0009(19)	0.012(2)	0.007(2)
P1	0.0352(4)	0.0346(4)	0.0347(4)	-0.0022(3)	0.0056(3)	0.0009(3)
P2	0.0424(5)	0.0349(4)	0.0387(4)	-0.0032(3)	0.0099(3)	-0.0026(3)
N4	0.0487(17)	0.0472(16)	0.0580(18)	-0.0020(14)	-0.0054(14)	-0.0006(13)
O4	0.110(3)	0.096(2)	0.086(2)	0.0297(19)	-0.027(2)	0.014(2)
C6	0.0411(17)	0.0309(14)	0.0371(15)	-0.0016(11)	0.0066(13)	-0.0006(12)
C8	0.0346(15)	0.0336(15)	0.0404(16)	-0.0039(12)	0.0062(13)	0.0016(12)
C9	0.054(2)	0.0346(15)	0.0354(15)	-0.0030(12)	0.0073(14)	-0.0008(14)
C10	0.0429(17)	0.0412(16)	0.0413(16)	-0.0053(13)	0.0103(13)	-0.0081(14)
C12	0.0395(17)	0.0360(16)	0.0490(18)	-0.0012(13)	0.0089(14)	0.0000()
C13	0.0414(17)	0.0510(19)	0.0365(16)	0.0003(13)	0.0075(13)	0.0034(14)
C14	0.0494(19)	0.0408(17)	0.0426(17)	-0.0012(13)	0.0143(14)	0.0040(14)
C15	0.0416(17)	0.0499(18)	0.0412(17)	-0.0036(14)	0.0098(14)	0.0050(14)
C16	0.052(2)	0.0419(18)	0.0503(19)	-0.001(14)	0.0090(16)	-0.0010(14)
C17	0.0423(19)	0.0461(19)	0.077(3)	-0.0120(17)	0.0068(17)	-0.0005(15)
C18	0.0438(18)	0.0399(16)	0.0521(18)	0.0023(14)	0.0158(15)	-0.0003(14)
C19	0.0402(18)	0.0416(17)	0.064(2)	0.0094(15)	0.0065(16)	0.0063(14)
C20	0.0430(19)	0.0443(18)	0.067(2)	0.0015(15)	0.0214(17)	0.0114(14)
C21	0.049(2)	0.0528(19)	0.0453(18)	0.0087(15)	0.0032(15)	0.0049(16)
C22	0.054(2)	0.070(2)	0.053(2)	-0.0046(17)	0.0170(17)	-0.0030(18)
C23	0.078(3)	0.057(2)	0.061(2)	0.0021(18)	0.006(2)	0.020(2)
C24	0.055(2)	0.049(2)	0.091(3)	-0.017(2)	-0.009(2)	-0.0119(18)
C25	0.068(2)	0.047(2)	0.066(2)	0.0070(17)	0.0218(19)	-0.0004(18)
C26	0.061(2)	0.064(2)	0.079(3)	-0.0019(2)	0.027(2)	-0.0210(19)
C27	0.056(2)	0.0403(17)	0.060(2)	-0.0050(15)	0.0197(17)	0.0050(15)
C28	0.082(3)	0.076(3)	0.0395(19)	-0.0003(18)	0.0038(19)	-0.014(2)
C29	0.104(4)	0.042(2)	0.073(3)	0.0182(18)	0.024(2)	0.008(2)
C30	0.127(4)	0.050(2)	0.053(2)	0.0058(17)	0.034(2)	0.002(2)
C31	0.066(2)	0.052(2)	0.049(2)	-0.0039(16)	0.0079(17)	-0.0030(17)
C32	0.094(3)	0.082(3)	0.061(3)	-0.024(2)	0.022(2)	0.17(3)
C33	0.054(2)	0.073(3)	0.107(4)	0.017(3)	0.036(3)	-0.003(2)
C34	0.093(3)	0.085(3)	0.046(2)	-0.019(2)	0.024(2)	-0.018(3)
C35	0.055(2)	0.059(2)	0.060(2)	-0.0043(18)	0.0059(18)	0.0102(18)
C36	0.071(3)	0.066(2)	0.050(2)	-0.0123(18)	0.0083(19)	0.013(2)

Table B.2. (Continue).

Atom	U_{11}	U_{22}	U_{33}	U_{23}	U_{13}	U_{12}
C37	0.074(3)	0.0401(18)	0.059(2)	-0.0137(16)	0.0032(19)	0.0016(18)
C39	0.062(3)	0.089(3)	0.070(3)	0.006(2)	0.029(2)	0.004(2)
C40	0.065(3)	0.080(3)	0.116(4)	-0.022(3)	0.028(3)	-0.030(2)
C41	0.095(3)	0.090(3)	0.052(2)	-0.017(2)	0.020(2)	-0.035(3)
C44	0.117(4)	0.133(5)	0.050(3)	-0.033(3)	0.019(3)	-0.031(4)
C46	0.174(6)	0.077(3)	0.066(3)	0.022(3)	0.050(3)	0.009(3)
C47	0.106(4)	0.131(5)	0.044(2)	0.012(3)	0.025(2)	0.017(3)

[a] Estimated standard deviations of the least significant digits are given in parentheses.

The form of the anisotropic function is:

$$U = \exp(-2\pi^2[h^2(a*)^2U_{11} + k^2(b*)^2U_{22} + l^2(c*)^2U_{33} + 2(hka*b*U_{12} + hla*c*U_{13} + klb*c*U_{23})]$$

Table B.3. Selected Interatomic Bond Lengths[a] (Å).

Atoms	Distance
Ni−P1	2.244(8)
Ni−P2	2.289(1)
Ni–N1	2.008(3)
Ni–N4	1.692(9)
N1–N2	1.150(5)
N2–N3	1.157(8)
N4–O1	1.129(0)

[a] Estimated standard deviations of the least significant digits are given in parentheses.

Table B.4. Selected Interatomic Bond Angles[a] (˚)

Atoms	Angle
P1–Ni–P2	120.90(7)
P1–Ni–N1	103.01(6)
P1–Ni–N4	101.22(6)
P1–Ni–N1	94.58(7)
P2–Ni–N4	109.91(6)
N1–Ni–N4	129.13(6)
Ni–N1–02	126.58(7)
Ni–N4–O1	152.72(7)
N1–N2–N3	173.71(7)
NiP2−NiN2	dihedral angle 84.73

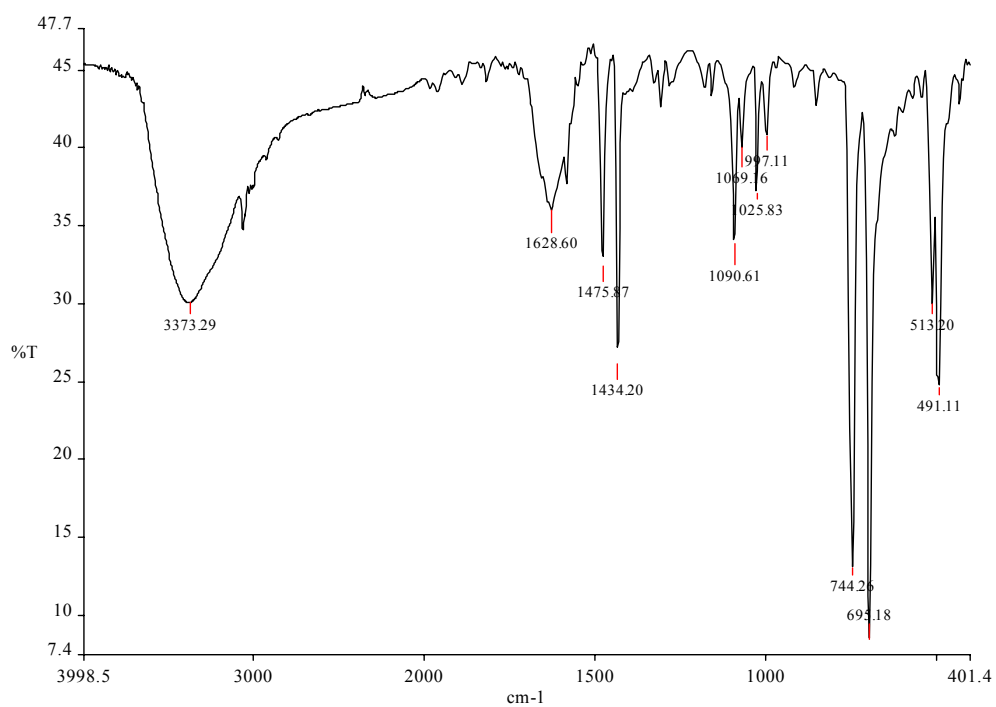[a] Estimated standard deviations of the least significant digits are given in parentheses.
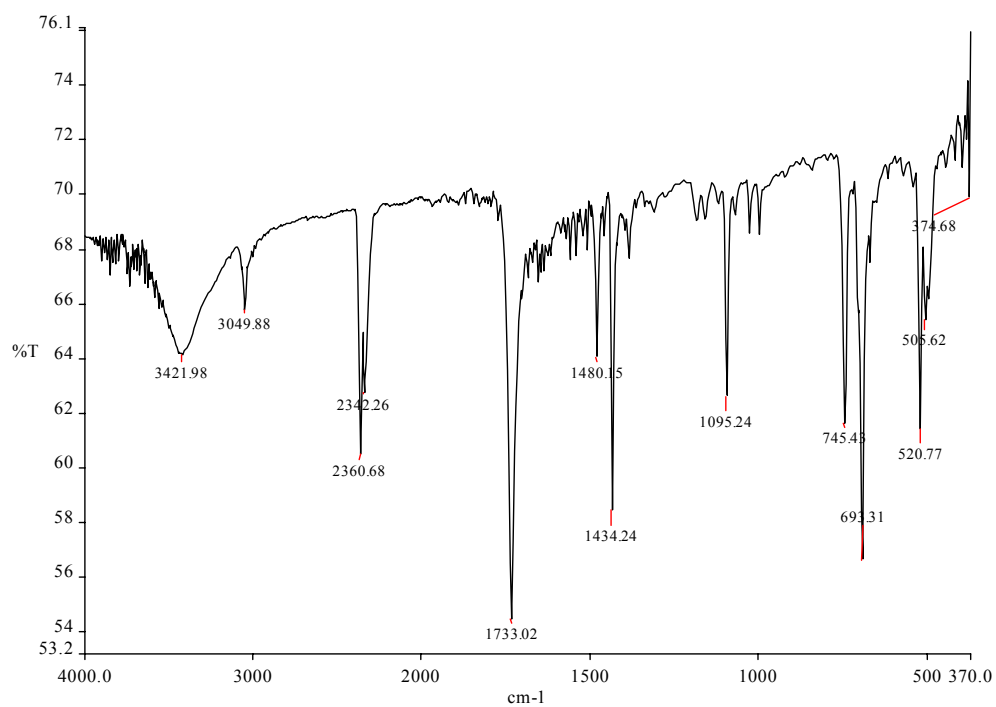
Figure B.1. FTIR spectrum of NiBr$_2$(PPh$_3$)$_2$
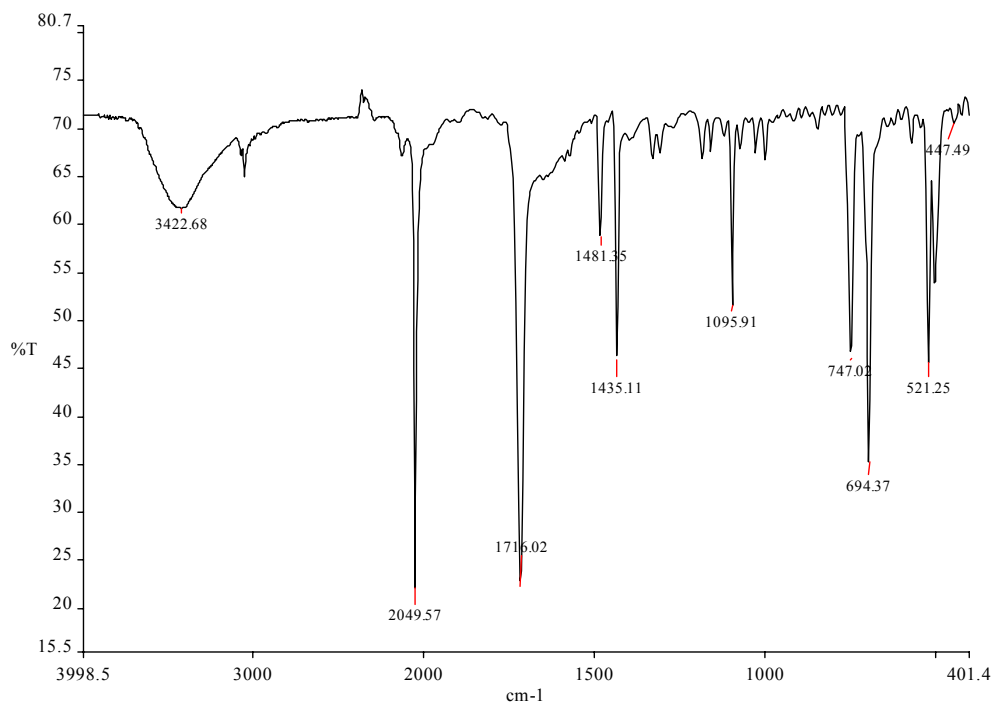

Figure B.2. FTIR spectrum of NiBr(NO)(PPh$_3$)$_2$

Figure B.3. FTIR spectrum of $Ni(N_3)(NO)(PPh_3)_2$

Table B.5. Description of the Short Intermolecular Phosphorus-Phosphorus Contacts for $NiN_3(NO)(PPh_3)_2$.

$Pn^A...Pn^s$	Primed Position (Pn^s)	Midpoint of $Pn^A...Pn^{s*}$	$Pn^A...Pn^s$ Distance (Å)	Ni- $Pn^A...Pn^s$ Angle (°)	$Pn^A...Pn^s$-Ni^s Angle (°)	Colinearity Parameter (°)
P1...P1^K	55504 (K)	(1.1246, 0.2500, 0.7318)	7.783	171.06	64.54	117.80
P1...P2^F	65602 (F)	(0.8362, 0.2929, 0.5082)	8.658	112.59	145.56	129.08
P1...P2^G	75703 (G)	(1.0862, 0.0868, 1.0082)	8.686	105.87	90.51	98.19
P1...P2^I	75603 (I)	(1.0862, 0.0868, 0.5082)	8.802	125.61	104.37	114.99
P1...P2^J	65603 (J)	(0.5862, 0.0868, 0.5082)	8.887	48.32	110.10	79.21
P1...P1^I	75603 (I)	(1, 0, 1/2)	8.945	100.98	100.98	100.98
P1...P2^K	55504 (K)	(1.0385, 0.3368, 0.7263)	8.934	145.89	32.59	89.24
P1...P1^G	75703 (G)	(1, 0, 1)	8.983	83.32	83.32	83.32
P2...P2^J	65603 (J)	(1/2, 0, 1/2)	7.350	86.98	86.98	86.98
P1...P1^M	45504 (M)	(0.6246, 0.2500, 0.7318)	7.783	64.54	171.06	117.80
P2...P1^E	64602 (E)	(0.6639, -0.2072, 0.4918)	8.658	145.56	112.59	129.08
P2...P1^G	75703 (G)	(0.9139, -0.0868, 0.9918)	8.686	90.51	105.87	98.19
P2...P1^I	75603 (I)	(0.9139, -0.0868, 0.4918)	8.802	104.37	125.61	114.99
P2...P1^J	65603 (J)	(0.4139, -0.0868, 0.4918)	8.887	110.10	48.32	79.21
P2...P1^M	45504 (M)	(0.5384, 0.1632, 0.7236)	8.934	32.59	145.89	89.24

Table B.6. Table of Symmetry Operations for $NiN_3(NO)(PPh_3)_2$.

Atom Designator Code(ADC)	Coordinate of Positions	Symbol of Symmetry Operation, s	Atom Designator Code(ADC)	Coordinate of Positions	Symbol of Symmetry Operation, s
55501	x, y, z	A	65703	-x+1, -y, -z+2	H
65501	x+1, y, z	B	75603	-x+2, -y, -z+1	I
45501	x-1, y, z	C	65603	-x+1, -y,-z+1	J
65702	-x+3/2, y+1/2, -z+2	D	55504	x+1/2, -y+1/2, z	K
64602	-x+3/2, y-1/2, -z+3/2	E	54504	x+1/2, -y-1/2, z	L
65602	-x+3/2, y+1/2, -z+3/2	F	45504	x-1/2, -y-1/2, z	M
75703	-x+2, -y, -z+2	G	44504	x-1/2, -y-1/2, z	N

APPENDIX C
ABSTRACTS AND PRESENTATIONS

1. Khosavithitkul, N. and Haller, K. J. Crystal and Molecular Structure of the Beta Form of L-Glutamic Acid. **The 3rd National Symposium on Graduate Research.** 18-19 August 2002, Suranaree University of Technology, Nakhon Ratchasima, Thailand.

2. Khosavithitkul, N. and Haller, K. J. Synthesis of the Four-Coordinate Azidonitrosylbis(triphenylphosphine)nickel. **The 29th Congress on Science and Technology of Thailand.** 20-22 October 2003, Golden Jubilee Convention Hall, Khon Kaen University, Thailand.

3. Khosavithitkul, N. and Haller, K. J. Supramolecular Structure of Azidonitrosylbis(triphenylphosphine)nickel. **The Sixth Conference of the Asian Crystallographic Association, AsCA'04.** 27-30 June 2004, Hong Kong University of Science and Technology, Hong Kong, China. (Poster Presentation).

4. Khosavithitkul, N. and Haller, K. J. Supramolecular Interactions in Four-Coordinate Azidonitrosylbis(triphenylphosphine)nickel. **The 11th Tri-University International Joint Seminar & Symposium 2003: Role of Asia in the World**. 26-31 October 2004, Chaing Mai, Thailand. (Oral Presentation).

CURRICULUM VITAE

NONGNAPHAT KHOSAVITHITKUL

Born: March 23, 1970, Nakhon Ratchasima, Thailand

Citizenship: Thai

Marital Status: Married

Degree:

1991   B.Sc., Chemistry,

              Prince of Songkhla University, Hatt Yai, Songkla, Thailand

2004   M. Sc., Chemistry

              Suranaree University of Technology, Nakhon Ratchasima, Thailand

Relevant Experience:

1995-Present Scientist

              The Center of Scientific and Technological

              Equipment, Suranaree University of Technology,

              Thailand

Publication:

Khosavithitkul, N. and Haller, K. J. Supramolecular Interactions in Four-Coordinate Azidonitrosylbis(triphenylphosphine)nickel. **The 11th Tri-University International Joint Seminar & Symposium 2003: Role of Asia in the World**. 26-31 October 2004, Chaing Mai, Thailand. pp 212-215.

Khosavithitkul, N., Kiatpichitpong, A. and Haller, K. J. Analyzing Concerted Noncovalent Interactions in Structures Dominated by Phenyl Rings. **The 9th Annual National Symposium on Computational Science & Engineering.** 23-25 March 2005, Mahidol University, Thailand. pp